Hybrid RIS With Sub-Connected Active Partitions: Performance Analysis and Transmission Design

Konstantinos Ntougias, *Member, IEEE*, Symeon Chatzinotas, *Fellow, IEEE*, and Ioannis Krikidis, *Fellow, IEEE*

***Abstract*—The emerging reflecting intelligent surface (RIS) technology promises to enhance the capacity of wireless communication systems via passive reflect beamforming. However, the product path loss limits its performance gains. Fully-connected (FC) active RIS, which integrates reflect-type power amplifiers into the RIS elements, has been recently introduced in response to this issue. Also, sub-connected (SC) active RIS and hybrid FC-active/passive RIS variants which employ a limited number of reflect-type power amplifiers, in order to provide energy savings, have been proposed. Nevertheless, their flexibility in balancing diverse capacity requirements and power consumption constraints is limited. In this direction, this study introduces novel hybrid RIS structures, wherein at least one reflecting sub-surface (RS) adopts the SC-active RIS design. The asymptotic signal-to-noise-ratio of the FC-active/passive and the proposed hybrid RIS variants is analyzed in a single-user single-input single-output setup. The transmit and RIS beamforming weights are jointly optimized in each scenario to maximize the energy efficiency of a hybrid RIS-aided multi-user multiple-input single-output downlink system subject to the power consumption constraints of the base station and the active RSs. Numerical simulation and analytic results highlight the performance gains of the proposed RIS designs over benchmarks, unveil non-trivial trade-offs, and provide valuable insights.**

***Index Terms*—Reflecting intelligent surface (RIS), hybrid RIS, beamforming, performance analysis, optimization.**

I. Introduction

The disruptive reflecting intelligent surface (RIS) technology has been recently proposed as a means to increase the data rates and the capacity, extend the coverage, and improve the reliability of wireless communication systems in a cost-effective and energy-efficient manner. This goal is accomplished by dynamically reconfiguring the wireless channel via reflect beamforming (RB) [1], [2]. Specifically, RIS refers to a planar surface that is equipped with a massive number of *passive* reflecting elements (RE). This intermediary can controllably reflect the incident radio frequency (RF) signal by jointly adjusting the phase shifts that the REs independently induce to it, thereby intelligently shaping the wireless propagation environment, e.g., to boost the received power at intended users or/and suppress the interference to other directions.

Nevertheless, the double path loss over the RIS-cascaded channels between the base station (BS) and the users, which equals the product of the path losses over the BS–RIS channel and the corresponding RIS–user channels, limits the capacity gains of passive RIS [3]. This is particularly apparent when the respective direct channels are strong. Despite its high RB gains, which are attributed to the vast volume of REs, RIS cannot effectively compensate for this multiplicative path loss.

A *fully-connected (FC) active* RIS alternative has been recently introduced to alleviate this performance bottleneck [4], [5]. In this RIS variant, a low-cost reflection-type power amplifier (PA), which is realized with the aid of an active load (negative resistance), such as a tunnel diode, is integrated into each RE. Hence, this RIS design supports both amplitude amplification and phase shifting of the incident signal prior to reflection, thus effectively mitigating the path loss effect over the BS–RIS channel without using costly RF chains.

A *sub-connected (SC) active* RIS structure, which is divided into disjoint partitions with their own reflection-type PA that is shared among their REs, constitutes a recent advancement that has been proposed to further enhance the energy efficiency (EE) [6]. Likewise, a hybrid RIS realization, consisting of an FC-active and a passive reflecting sub-surface (RS), represents yet another recent development, in an attempt to flexibly combine the advantages of these RIS architectures and strike a desirable capacity/total power consumption (TPC) balance [7].

A. Related Works

Numerous studies have explored the joint optimization of the transmit and reflect beamforming schemes in a multitude of diverse RIS-aided wireless communication scenarios.

Passive RIS: The works [8], [9] deal with capacity maximization in point-to-point multiple-input single-output (MISO) and multiple-input multiple-output (MIMO) systems, respectively. The studies [10], [11] address transmit sum-power (TSP) minimization in the multi-user MISO downlink scenario, whereas [12] extends these works for the case with discrete reflection coefficients (RC). The study [13] proposes a respective worst-case robust algorithm under a scenario where only the RIS–user reflection channels are imperfectly known, while [14] focuses on outage-constrained robust designs under spectrum sharing and energy harvesting constraints. Sum-rate (SR) and EE maximization are investigated in [3], [15], respectively, under the application of zero-forcing precoding. The work [16] explores weighted SR (WSR) maximization and [17] studies a corresponding robust design, assuming the ability to control the reflection amplitudes as well.

These works corroborate the advantages of RIS-aided communication over benchmarks, such as full-duplex active relays, and emphasize the importance of optimizing the phase shifts in order to exploit coherent RB gains, rather than relying on random phase shifts which solely provide array gains.

FC-active RIS: An optimal power allocation scheme that maximizes the data rate in a single-user single-input single-output (SISO) system is presented in [4]. In [18], [19], the

authors jointly optimize the reflect and receive beamforming or the transmit precoding (TP) and RB schemes in a single-user single-input multiple-output (SIMO) or a multi-user MISO downlink system to maximize the received signal-to-noise-ratio (SNR) or to minimize the TSP, respectively. The work [20] focuses instead on SR maximization.

According to these studies, this RIS architecture outperforms its passive counterpart under the same TPC budget, provided that the number of REs and, therefore, reflect-type PAs is relatively small, due to TPC considerations.

SC-active and FC-active/passive RIS: The authors in [6] develop a joint TP/RB optimization scheme that maximizes the EE in an SC-active RIS-aided multi-user MISO downlink system. Numerical simulations unveil that this active RIS variant provides significant TPC savings in comparison to the FC-active RIS design, with only a minimal SR deterioration.

The authors in [7], in turn, consider an FC-active/passive RIS-assisted multi-user MISO downlink system and jointly optimize the TP and RB schemes, along with the allocation of active and passive REs, to maximize the ergodic capacity of the worst-case user under the availability of statistical CSI. Numerical evaluations indicate that smaller TPC budgets and stronger direct links benefit active over passive REs. In [21] the authors consider a corresponding unmanned aerial vehicle-aided communication system and optimize also the location of the, static, drone under the max-min fairness objective, whereas in [22] they extend this work by assuming a moving drone and optimizing its trajectory. The work [23], on the other hand, focuses on EE maximization in a cell-free network and corroborates the superiority of this hybrid RIS design over passive and active RIS.

B. Motivation and Goal

Nowadays, we notice an urgency to reduce the TPC and the carbon footprint of wireless networks and enhance their EE, in view of both their densification, which is dictated by their ambitious capacity targets, and rising sustainability challenges, such as the energy crisis and the climate change [24].

Although the SC-active [6] and FC-active/passive [7] RIS variants correspond to steps in the right direction, their ability of simultaneously satisfying diverse capacity requirements and TPC constraints is limited. Motivated by these works, our main goal is to progress the state-of-the-art by introducing flexible and energy-efficient RIS designs that combine the hybrid RIS principle with the degrees-of-freedom offered by SC-active RIS regarding the number of RIS partitions (i.e., PAs).

C. Contributions

The unique contributions of this study are listed below:

- We analyze the asymptotic SNR of the proposed hybrid RIS architectures and the FC-active/passive RIS variant in an IRS-aided single-user SISO downlink system, as the number of REs grows to infinity.
- We jointly optimize the TP and RB schemes for each scenario, such that the EE of an IRS-aided multi-user MISO downlink system is maximized subject to the TPC constraints of the BS and any active RS. We apply fractional programming (FP) techniques and develop efficient block coordinate ascent (BCA) algorithms based on the Lagrange multipliers and majorization-minimization (MM) methods to tackle these challenging non-convex optimization problems and obtain locally optimal solutions.
- We comparatively evaluate the proposed schemes against benchmarks in various test scenarios via simulations.

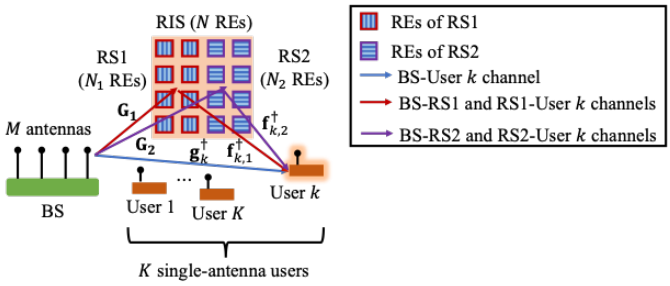

Fig. 1. System setup: a RIS-assisted multi-user MISO downlink system, wherein a hybrid RIS with N REs that is divided into two RSs, RS1 and RS2, with N_1 and N_2 REs, respectively, aids a BS with M antennas in serving K single-antenna users in a single time-frequency resource. The figure also depicts the direct channel from the BS to user k, the incident channels from the BS to each RS, and the reflected channels from each RS to user k.

Numerical simulation and analytic results showcase the performance gains of the proposed designs over the state-of-the-art and shed light on the impact of system parameters.

D. Structure, Mathematical Notation, and Abbreviations

The rest of the paper is organized as follows: The considered hybrid RIS architectures and the system model are introduced in Section II. Section III is devoted to performance analysis. In Section IV, the joint TP/RB optimization problems for each scenario are formulated and respective energy-efficient designs are proposed. In Section V, the performance of the proposed schemes is comparatively evaluated against benchmarks via numerical simulations. Section VI summarizes the paper and presents our primary conclusions.

Notation: x: a scalar; $\mathbf{x}$: a column vector; $\mathbf{X}$: a matrix; $[\mathbf{x}]_n \triangleq x_n$: the n-th element of $\mathbf{x}$; $\mathbb{R}_+$: the set of non-negative real numbers; $\mathbb{C}^N$ and $\mathbb{C}^{N\times M}$: the sets of complex $N \times 1$ vectors and $N \times M$ matrices, respectively; $\mathbb{B}^{N\times M}$: the set of binary $N \times M$ matrices; $j \triangleq \sqrt{-1}$: the imaginary unit; $|x|$, $\arg(x)$, and $\mathrm{Re}\{x\}$: the magnitude, argument, and real part, respectively, of the complex scalar x; $\|\mathbf{x}\|$: the Euclidean norm of $\mathbf{x}$; $\mathbf{X}^*$, $\mathbf{X}^T$, $\mathbf{X}^\dagger$, $\mathbf{X}^{-1}$, and $\|\mathbf{X}\|_F$: the complex conjugate, transpose, complex conjugate transpose, inverse, and Frobenius norm of $\mathbf{X}$, respectively; $\mathbf{X} = \mathrm{diag}(\mathbf{x})$: a diagonal matrix with main diagonal $\mathbf{x} = \mathrm{Diag}(\mathbf{X})$; $\mathbf{X} = \mathrm{blockdiag}(\mathbf{X}_1, \ldots, \mathbf{X}_L)$: a block diagonal matrix; $\mathbf{X} \succeq \mathbf{0}$: a positive semi-definite (PSD) matrix; $\mathbf{0}_N$ and $\mathbf{1}_N$: the $N \times 1$ null and all-ones vector, respectively; $\mathbf{I}_N$: the $N \times N$ identity matrix; $\otimes$ and $\odot$: the Kronecker and Handamard matrix product, respectively; $\mathbb{E}\{\cdot\}$: the expectation operator; $\mathcal{CN}(\cdot,\cdot)$: the circularly symmetric complex Gaussian distribution.

Abbreviations: The abbreviations are listed in Table I.

TABLE I
ABBREVIATIONS

Abbreviation	Description	Abbreviation	Description
AF	Amplification Factor	QCQP	Quadratically-Constrained Quadratic Program
AWGN	Additive White Gaussian Noise	RB	Reflect Beamforming
BCA	Block Coordinate Ascent	RC	Reflection Coefficient
BS	Base Station	RE	Reflection Element
CSI	Channel State Information	RF	Radio Frequency
DC	Direct Current	RIS	Reflecting Intelligent Surface
EE	Energy Efficiency	RS	Reflecting Sub-surface
FC/SC	Fully-/Sub-Connected	SIMO/SISO	Single-Input Multiple-/Single-Output
FP	Fractional Programming	S(I)NR	Signal-to-(Interference-plus)-Noise-Ratio
MIMO/MISO	Multiple-Input Multiple-/Single-Output	TP	Transmit Precoding
MM	Majorization-Minimization	TPC	Total Power Consumption
OF	Objective Function	TSP	Transmit Sum-Power
PA	Power Amplifier	UE	User Equipment
PS	Phase Shifts	UMC	Unit Modulus Constraints
PSD	Positive Semi-Definite	(W)SR	(Weighted) Sum-Rate

II. Hybrid RIS Structures and System Model

A. System Setup

The considered setup consists of a BS with M antennas, a hybrid RIS with N REs, and a set $\mathcal{K} \triangleq \{1, \ldots, K\}$ of single-antenna terminals, as shown in Fig. 1. The RIS is divided into two RSs with a set $\mathcal{N}_s \triangleq \{1, \ldots, N_s\}$ of REs each, $s \in \mathcal{S} \triangleq \{1, 2\}$, such that $N_1 + N_2 = N$. RS s employs the passive, the FC-active, or the SC-active RIS design, which are illustrated in Fig. 2. In the latter case, it is divided into a set $\mathcal{L}_s \triangleq \{1, \ldots, L_s\}$ of partitions with $T_s = N_s/L_s$ REs each. Throughout the paper, we address the members of these sets via the indexes $n \in \mathcal{N}_s$, $l \in \mathcal{L}_s$, and $k, i \in \mathcal{K}$, respectively.

B. Hybrid RIS Architectures and RB Matrix

We consider active/passive and active/active RIS architectures. Specifically, besides the FC-active/passive structure [7], we propose the SC-active/passive, FC-active/SC-active, and SC-active/SC-active (with $L_1 \neq L_2$ or/and $N_1 \neq N_2$) variants, as depicted in Fig. 2. The RB matrix of the hybrid RIS, $\boldsymbol{\Phi} \in \mathbb{C}^{N \times N}$, and RS s, $\boldsymbol{\Phi}_s \in \mathbb{C}^{N_s \times N_s}$, is expressed as $\boldsymbol{\Phi} = \text{blockdiag}\left(\boldsymbol{\Phi}_1, \boldsymbol{\Phi}_2\right)$ and $\boldsymbol{\Phi}_s = \text{diag}\left(\phi_{1,s}, \ldots, \phi_{N_s,s}\right)$, respectively, where $\phi_{n,s} \in \mathbb{C}$ corresponds to the RC of the n-th RE in RS s. Depending on the RS type,

$$\phi_{n,s} = e^{j\theta_{n,s}} \Rightarrow \boldsymbol{\Phi}_s \triangleq \boldsymbol{\Theta}_s \text{ (Passive RS)}, \tag{1a}$$

$$\phi_{n,s} = \alpha_{n,s} e^{j\theta_{n,s}} \Rightarrow \boldsymbol{\Phi}_s \triangleq \boldsymbol{\Theta}_s \mathbf{A}_s \text{ (FC-Active RS)} \tag{1b}$$

$$\phi_{n,s} = \widetilde{\alpha}_{l,s} e^{j\theta_{n,s}},\ (l-1)\,T_s \leq n \leq l T_s \Rightarrow$$
$$\Rightarrow \boldsymbol{\Phi}_s \triangleq \boldsymbol{\Theta}_s\, \text{diag}\left(\boldsymbol{\Gamma}_s \widetilde{\boldsymbol{\alpha}}_s\right) \text{ (SC-Active RS)}, \tag{1c}$$

where $\theta_{n,s} \in [0, 2\pi)$ and $\alpha_{n,s} \geq 0$ denote the phase shift (PS) and the amplification factor (AF), respectively, of the n-th RE; $\boldsymbol{\Theta}_s \in \mathbb{C}^{N_s \times N_s}$ is referred to as the PSs matrix; $\mathbf{A}_s \in \mathbb{R}_+^{N_s \times N_s}$ stands for the AFs matrix, $\mathbf{A}_s \triangleq \text{diag}\left(\alpha_{1,s}, \ldots, \alpha_{N_s,s}\right)$; $\widetilde{\boldsymbol{\alpha}}_s \in \mathbb{R}_+^{L_s}$ represents the AFs vector for the SC-active RS case, $\widetilde{\boldsymbol{\alpha}}_s \triangleq \left[\widetilde{\alpha}_{1,s}, \ldots, \widetilde{\alpha}_{L_s,s}\right]^T$, with $\widetilde{\alpha}_{l,s} \geq 0$ standing for the AF of the l-th partition; and $\boldsymbol{\Gamma}_s \in \mathbb{B}^{N_s \times L_s}$ denotes the coupling matrix, $\boldsymbol{\Gamma}_s \triangleq \mathbf{I}_{L_s} \otimes \mathbf{1}_{T_s}$ [6]. Note that passive RS is a special case of FC-active RS with $\alpha_{n,s} = 1$, $\forall n \in \mathcal{N}_s$, i.e., $\mathbf{A}_s = \mathbf{I}_{N_s}$. Likewise, FC-active RS is a special case of SC-active RS with $T_s = 1$, such that $L_s = N_s$, i.e., $\text{diag}\left(\boldsymbol{\Gamma}_s \widetilde{\boldsymbol{\alpha}}_s\right) = \mathbf{A}_s$.

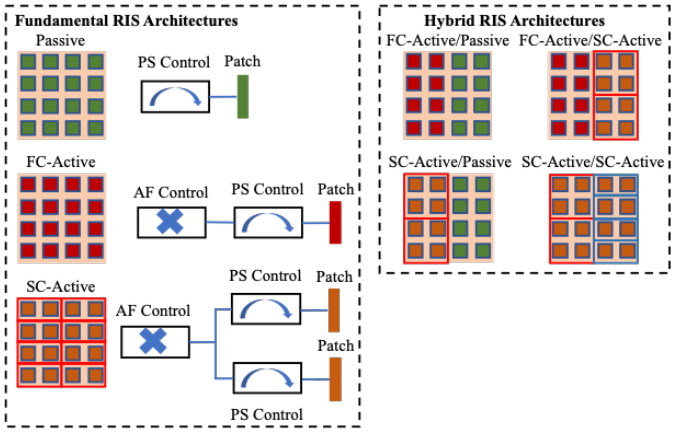

Fig. 2. Fundamental and hybrid RIS architectures. In all fundamental RIS structures, we have PS control for each RE (patch). In FC-active and SC-active RS, we also have AF control per RE or disjoint partition (subgroup of REs), respectively. By combining either active RS design with either a passive or SC-active RS, we obtain four hybrid RIS variants, i.e., two active/passive and two active/active ones.

C. Channel Model

We consider quasi-static, flat-fading channels. The baseband equivalent direct channel from the BS to user k, incident channel from the BS to RS s, and reflected channel from RS s to user k is denoted by $\mathbf{g}_k^\dagger \in \mathbb{C}^M$, $\mathbf{G}_s \in \mathbb{C}^{N_s \times M}$, and $\mathbf{f}_{k,s}^\dagger \in \mathbb{C}^{N_s}$, respectively. The baseband equivalent effective channel from the BS to user k, $\mathbf{h}_k^\dagger \in \mathbb{C}^M$, is given by $\mathbf{h}_k^\dagger \triangleq \mathbf{g}_k^\dagger + \sum_{s \in \mathcal{S}} \mathbf{f}_{k,s}^\dagger \boldsymbol{\Phi}_s \mathbf{G}_s$.

D. Transmitted Signals

The transmitted signal, $\mathbf{x} \in \mathbb{C}^M$, is $\mathbf{x} = \sum_{k \in \mathcal{K}} \mathbf{w}_k s_k$, where $\mathbf{w}_k \in \mathbb{C}^M$ and $s_k \sim \mathcal{CN}(0, 1)$ are the TP vector and data symbol, respectively, for user k. The TSP is written as

$$P_t = \mathbb{E}\left\{\|\mathbf{x}\|^2\right\} = \sum_{k \in \mathcal{K}} \|\mathbf{w}_k\|^2. \tag{2}$$

E. Total Power Consumption

Depending on whether RS s is active or passive, the amplified and reflected or simply reflected signal, $\mathbf{t}_s \in \mathbb{C}^{N_s}$,

is written as $\mathbf{t}_s = \mathbf{\Phi}_s(\mathbf{r}_s + \mathbf{z}_s)$ or $\mathbf{t}_s = \mathbf{\Phi}_s\mathbf{r}_s$, respectively, where $\mathbf{r}_s \in \mathbb{C}^{N_s}$ denotes the incident RF signal given by $\mathbf{r}_s = \mathbf{G}_s\mathbf{x}$ and $\mathbf{z}_s \sim \mathcal{CN}\left(\mathbf{0}_{N_s}, \delta_s^2\mathbf{I}_{N_s}\right)$ represents the active RS's amplification noise. The TSP of active RS s is given by

$$P_{r,s} = \mathbb{E}\left\{\|\mathbf{t}_s\|^2\right\} = \sum_{k\in\mathcal{K}} \|\mathbf{\Phi}_s\mathbf{G}_s\mathbf{w}_k\|^2 + \delta_s^2\|\mathbf{\Phi}_s\|_F^2. \quad (3)$$

The TPC of the BS, user equipment (UE), and RS s is

$$P_{\text{BS}} = \xi^{-1}P_t + W_{\text{BS}},\ P_{\text{UE}} = \sum_{k\in\mathcal{K}} W_{\text{UE}}, \quad (4a)$$

$$P_s = N_sP_{\text{PS}},\ \text{(Passive RS)} \quad (4b)$$

$$P_s = \zeta_s^{-1}P_{r,s} + W_{r,s},\ \text{(Active RS)} \quad (4c)$$

where W_{BS} and $W_{r,s}$ respectively refer to the static power consumption of BS and RS s, $\xi \in (0,1)$ and $\zeta_s \in (0,1)$ is the EE of their amplifiers, W_{UE} and P_{PS} denote the power consumption of each UE and PS control circuit, respectively. If RS s is active, then

$$W_{r,s} = N_s\left(P_{\text{PS}} + P_{\text{DC}}\right),\ \text{(FC-active RS)} \quad (5a)$$

$$W_{r,s} = N_sP_{\text{PS}} + \left(N_s/T_s\right)P_{\text{DC}},\ \text{(SC-active RS)} \quad (5b)$$

where P_{DC} denotes the direct current (DC) bias of each PA. The TPC constraint of the BS and active RS s is given by $P_{\text{BS}} \le P_{\text{BS}}^{\max}$ and $P_s \le P_s^{\max}$, respectively, where $P_{\text{BS}}^{\max} > 0$ and $P_s^{\max} > 0$ denote the corresponding TPC budgets. By denoting $P_{\text{RIS}} \triangleq \sum_{s\in\mathcal{S}} P_s$ and $\widetilde{P} \triangleq P_{\text{BS}} + P_{\text{UE}}$, we can write the TPC of the system as $P = \widetilde{P} + P_{\text{RIS}}$.

F. Received Signals and SINR

Hybrid Active/Passive RIS: When the RIS adopts the FC-active/passive design presented in [7] or the proposed SC-active/passive one, the received signal at user k is given by

$$\begin{aligned} y_k =& \mathbf{g}_k^\dagger\mathbf{x} + \sum_{s\in\mathcal{S}} \mathbf{f}_{k,s}^\dagger\mathbf{t}_s + n_k \\ =& \underbrace{\mathbf{h}_k^\dagger\mathbf{w}_k s_k}_{\text{desired signal}} + \underbrace{\mathbf{h}_k^\dagger \sum_{i\in\mathcal{K}\setminus\{k\}} \mathbf{w}_i s_i}_{\text{multi-user interference}} + \underbrace{\mathbf{f}_{k,1}^\dagger\mathbf{\Phi}_1\mathbf{z}_1}_{\text{RS1 amplification noise}} + n_k, \end{aligned} \quad (6)$$

where $n_k \sim \mathcal{CN}\left(0, \sigma_k^2\right)$ denotes the additive white Gaussian noise (AWGN). Hence, the signal-to-interference-plus-noise-ratio (SINR) of this user is written as

$$\gamma_k = \frac{\left\|\mathbf{h}_k^\dagger\mathbf{w}_k\right\|^2}{\sum\limits_{i\in\mathcal{K}\setminus\{k\}} \left\|\mathbf{h}_k^\dagger\mathbf{w}_i\right\|^2 + \delta_1^2\left\|\mathbf{f}_{k,1}^\dagger\mathbf{\Phi}_1\right\|^2 + \sigma_k^2}. \quad (7)$$

Hybrid Active RIS: When the RIS adopts the proposed FC-/SC-active structure or consists of two SC-active RSs with different partitioning, the received signal at user k is given by

$$\begin{aligned} y_k =& \mathbf{g}_k^\dagger\mathbf{x} + \sum_{s\in\mathcal{S}} \mathbf{f}_{k,s}^\dagger\mathbf{t}_s + n_k \\ =& \underbrace{\mathbf{h}_k^\dagger\mathbf{w}_k s_k}_{\text{desired signal}} + \underbrace{\mathbf{h}_k^\dagger \sum_{i\in\mathcal{K}\setminus\{k\}} \mathbf{w}_i s_i}_{\text{multi-user interference}} + \underbrace{\sum_{s\in\mathcal{S}} \mathbf{f}_{k,s}^\dagger\mathbf{\Phi}_s\mathbf{z}_s}_{\text{RSs' amplification noise}} + n_k. \end{aligned} \quad (8)$$

Therefore, the SINR of this user is expressed as

$$\gamma_k = \frac{\left\|\mathbf{h}_k^\dagger\mathbf{w}_k\right\|^2}{\sum\limits_{i\in\mathcal{K}\setminus\{k\}} \left\|\mathbf{h}_k^\dagger\mathbf{w}_i\right\|^2 + \sum\limits_{s\in\mathcal{S}} \delta_s^2\left\|\mathbf{f}_{k,s}^\dagger\mathbf{\Phi}_s\right\|^2 + \sigma_k^2}. \quad (9)$$

G. Sum-Rate and Energy Efficiency

The data rate of user k and the SR (in bps/Hz) are respectively given by $R_k = \log_2(1+\gamma_k)$ and $R = \sum_{k\in\mathcal{K}} R_k$, while the EE of the system is written as $\eta = R/P$.

III. Performance Analysis

In this section, we analyze the asymptotic SNR of the considered hybrid RIS architectures as $N_s \to \infty$. We consider a single-user RIS-aided SISO communication setup, i.e., $M = K = 1$, with Rayleigh-fading incident BS–RS s channel, $\mathbf{g}_s \in \mathbb{C}^{N_s}$, and reflected RS s–user channel, $\mathbf{f}_s^\dagger \in \mathbb{C}^{N_s}$, i.e., $\mathbf{g}_s \sim \mathcal{CN}\left(\mathbf{0}_{N_s}, \varrho_{g_s}^2\mathbf{I}_{N_s}\right)$ and $\mathbf{f}_s \sim \mathcal{CN}\left(\mathbf{0}_{N_s}, \varrho_{f_s}^2\mathbf{I}_{N_s}\right)$, respectively, to foster mathematical tractability and obtain insights about the respective power scaling laws. For the same purpose, we also assume that the direct BS-user link is blocked, such that the effective channel from the BS to the user, $h^* \in \mathbb{C}$, is defined as $h^* \triangleq \sum_{s\in\mathcal{S}} \mathbf{f}_s^\dagger\mathbf{\Phi}_s\mathbf{g}_s$, and assume that if RS s is active, then all its AFs are equal. This implies an SC-active RS with a single PA (i.e., $L = 1$), such that $\widetilde{\alpha}_{l,s} = \widetilde{\alpha}_s$, $\forall l \in \mathcal{L}_s$. This configuration has been proven to be optimal for single-user SISO [6]. The transmit power budget and the reflect power budget of active RS s are denoted by $P_{t,a/p}^{\max}$ or $P_{t,a/a}^{\max}$ for the active/passive or active/active RIS case and $P_{r,s}^{\max}$, respectively, while the AWGN is denoted as $n \sim \mathcal{CN}\left(0, \sigma^2\right)$. The transmitted signal is denoted by $x = ws$, where $w \ge 0$ and $s \sim \mathcal{CN}(0,1)$ represent the transmit power and the transmitted symbol, respectively. Furthermore, we assume optimal transmit power, AFs, and PSs.

For comparison purposes, we also consider the passive and single-PA-equipped active RIS designs as $N \to \infty$. The incident BS–RIS and reflected RIS–user channel are denoted in these scenarios as $\mathbf{g} \sim \mathcal{CN}\left(\mathbf{0}_N, \varrho_g^2\mathbf{I}_N\right)$ and $\mathbf{f} \sim \mathcal{CN}\left(\mathbf{0}_N, \varrho_f^2\mathbf{I}_N\right)$, respectively; the transmit and reflect power budgets are denoted as $P_{t,p}^{\max}$ or $P_{t,a}^{\max}$ for the passive or active RIS case and $P_r^{\max}$, respectively; and the amplification noise of the active RIS is denoted as $\mathbf{z} \sim \mathcal{CN}\left(\mathbf{0}_N, \delta^2\mathbf{I}_N\right)$.

Throughout this section, we use the numeric example shown in Table II, which is adapted from [20]. Note that the total radiated power budget, $P_{\max}$, is the same in all setups, to ensure fair comparison. The numerical results regarding the asymptotic SNR and the minimum RIS size required to meet a given condition are presented in Tables III and IV, respectively.

A. Asymptotic SNR

First, we present the asymptotic SNR of the considered RIS-aided single-user SISO system for the different RIS types.

Lemma 1 (Asymptotic SNR for passive RIS): Letting $N \to \infty$, the asymptotic SNR of passive RIS is given by

$$\gamma_p\left(N, P_{t,p}^{\max}\right) \to N^2\frac{P_{t,p}^{\max}\pi^2\varrho_f^2\varrho_g^2}{16\sigma^2}. \quad (10)$$

TABLE II
PARAMETERS OF NUMERIC EXAMPLE

Parameter	Value	Notes
AWGN Power	$\sigma^2 = -100$ dBm	
Amplification Noise Power	$\delta^2 = -100$ dBm (Fundamental RIS Structure) $\delta_s^2 = -100$ dBm (RS s of Hybrid RIS)	
BS–RIS Path Loss	$\varrho_f^2 = -70$ dB (Fundamental RIS Structure) $\varrho_{f_s}^2 = -70$ dB (RS s of Hybrid RIS)	
RIS–User Path Loss	$\varrho_g^2 = -70$ dB (Fundamental RIS Structure) $\varrho_{g_s}^2 = -70$ dB (RS s of Hybrid RIS)	
Transmit Power Budget	$P_{t,p}^{\max} = P_{\max}$ (Passive RIS) $P_{t,a}^{\max} = P_{\max}/2$ (Active RIS) $P_{t,a/p}^{\max} = P_{\max}/2$ (Active/Passive RIS) $P_{t,a/a}^{\max} = P_{\max}/2$ (Active/Active RIS)	(i) $P_{t,p}^{\max} = 2$ W, (ii) $P_{t,p}^{\max} = 3$ W (i) $P_{t,a}^{\max} = 1$ W, (ii) $P_{t,a}^{\max} = 1.5$ W (i) $P_{t,a/p}^{\max} = 1$ W, (ii) $P_{t,a/p}^{\max} = 1.5$ W (i) $P_{t,a/a}^{\max} = 1$ W, (ii) $P_{t,a/a}^{\max} = 1.5$ W
Reflect Power Budget	$P_r^{\max} = P_{\max}/2$ (Active RIS) $P_{r,1}^{\max} = P_{\max}/2$ (RS1 of Active/Passive RIS) $P_{r,s}^{\max} = P_{\max}/2S$ (RS s of Active/Active RIS)	(i) $P_r^{\max} = 1$ W, (ii) $P_r^{\max} = 1.5$ W (i) $P_{r,1}^{\max} = 1$ W, (ii) $P_{r,1}^{\max} = 1.5$ W (i) $P_{r,s}^{\max} = 0.5$ W ($S = 2$) or $P_{r,s}^{\max} = 0.25$ W ($S = 4$), (ii) $P_{r,s}^{\max} = 0.75$ W ($S = 2$) or $P_{r,s}^{\max} = 0.375$ W ($S = 4$)
Total Radiated Power Budget	(i) $P_{\max} = 2$ W, (ii) $P_{\max} = 3$ W (50% increase)	$P_{\max} = P_{t,p}^{\max}$ (Passive RIS) $P_{\max} = P_{t,a}^{\max} + P_r^{\max}$ (Active RIS) $P_{\max} = P_{t,a/p}^{\max} + P_{r,1}^{\max}$ (Active/Passive RIS) $P_{\max} = P_{t,a/a}^{\max} + \sum_{s\in\mathcal{S}} P_{r,s}^{\max}$ (Active/Active RIS)
Number of REs	$N = 256$ (Fundamental RIS Structures) $N = N_1 + N_2 = 256$ (Hybrid RIS structures) Case 1: $N_1 = 3N/4 = 192$, $N_2 = N/4 = 64$. Case 2: $N_1 = N_2 = N/2 = 128$. Case 3: $N_1 = N/4 = 64$, $N_2 = 3N/4 = 192$.	Cases 1–3 apply to active/passive RIS. In active/active RIS, $N_s = N/S$, i.e., $N_s = 128$ ($S = 2$) or $N_s = 64$ ($S = 4$). 33% (50%) and 50% (33%) drop (increase) in active (passive) REs from Case 1 to 2 and then to 3.

Proof: The proof can be found in [10]. □

Remark 1: We notice that passive RIS enables a transmit power reduction in the order of N^2 without compromising the received SNR. This is because it does not only achieve a beamforming gain of order N in the RIS-user link, similar to its massive MIMO counterpart, but it also inherently captures an aperture gain of order N in the BS–RIS link [10].

Lemma 2 (Asymptotic SNR for active RIS): Letting $N \to \infty$, the asymptotic SNR for the active RIS case is given by

$$\gamma_a\left(N, P_{t,a}^{\max}, P_r^{\max}\right) \to N\frac{P_{t,a}^{\max}P_r^{\max}\pi^2\varrho_f^2\varrho_g^2}{16\left(P_r^{\max}\delta^2\varrho_f^2 + P_{t,a}^{\max}\sigma^2\varrho_g^2 + \sigma^2\delta^2\right)}. \tag{11}$$

Proof: The proof can be found in [20]. □

Remark 2: We observe that the asymptotic SNR of active RIS is only proportional to N, instead of N^2. Also, it depends on both the transmit power and amplification power budgets.

Remark 3: We note that

$$\gamma_a\left(N, P_{t,a}^{\max}, P_r^{\max}\right) \to \gamma_p\left(N, P_{t,a}^{\max}\right)\frac{P_r^{\max}\sigma^2}{N\left(P_r^{\max}\delta^2\varrho_f^2 + P_{t,a}^{\max}\sigma^2\varrho_g^2 + \sigma^2\delta^2\right)}. \tag{12}$$

Remark 4: By letting $P_{t,a}^{\max} \to \infty$ in Eq. (11), the asymptotic SNR of active RIS is upper-bounded by

$$\gamma_a^{\infty_t}\left(N, P_r^{\max}\right) \to N\frac{P_r^{\max}\pi^2\varrho_f^2}{16\sigma^2}. \tag{13}$$

By letting $P_r^{\max} \to \infty$ in Eq. (11), the asymptotic SNR of active RIS is upper-bounded by

$$\gamma_a^{\infty_r}\left(N, P_{t,a}^{\max}\right) \to N\frac{P_{t,a}^{\max}\pi^2\varrho_g^2}{16\delta^2}. \tag{14}$$

Hence, the negative impact of small BS–RIS channel $\mathbf{G}$ and large RIS noise power δ^2 or small RIS–user channel $\mathbf{f}$ and large AWGN power σ^2 on the received SNR can be reduced by increasing the transmit or the reflect power, as shown in Eqs. (13) and (14), respectively [20].

Remark 5: Active RIS achieves about 40 dB higher asymptotic SNR than passive RIS, as shown in Table III. This is due to the amplification power in the nominator of Eq. (11), which implies that active RIS compensates for the path loss in the BS–RIS channel, and the small multiplicative terms in the denominator of Eq. (11) that involve path loss and noise components, e.g., we see that the received RIS noise terms have been attenuated over the RIS–user channels. Also, 50% increase of $P_{\max}$ results in an SNR gain of $10\log_{10}(1.5) = 1.76$ dB for both RIS structures, while the transition of active RIS to the large transmit or reflect power regime results in an SNR gain of 3.01 dB.

Lemma 3 (Asymptotic SNR for active/passive RIS): Letting $N_s \to \infty$, the asymptotic SNR for the active/passive RIS case with arbitrary REs' allocation is given by

$$\begin{aligned}&\gamma_{a/p}\left(N, P_{t,a/p}^{\max}, P_{r,1}^{\max}\right) \to \\ &\frac{P_{t,a/p}^{\max}\pi^2\left[P_{r,1}^{\max}\varrho_{f_1}^2\varrho_{g_1}^2N_1 + \varrho_{f_2}^2\varrho_{g_2}^2\left(P_{t,a/p}^{\max}\varrho_{g_1}^2 + \delta_1^2\right)N_2^2\right]}{16\left(P_{r,1}^{\max}\delta_1^2\varrho_{f_1}^2 + P_{t,a/p}^{\max}\sigma^2\varrho_{g_1}^2 + \sigma^2\delta_1^2\right)} \\ &= \gamma_a\left(N_1, P_{t,a/p}^{\max}, P_{r,1}^{\max}\right) \\ &+ \gamma_p\left(N_2, P_{t,a/p}^{\max}\right)\frac{\left(\varrho_{g_1}^2P_{t,a/p}^{\max} + \delta_1^2\right)\sigma^2}{P_{t,a/p}^{\max}\left(P_{r,1}^{\max}\delta_1^2\varrho_{f_1}^2 + P_{t,a/p}^{\max}\sigma^2\varrho_{g_1}^2 + \sigma^2\delta_1^2\right)}.\end{aligned} \tag{15}$$

Proof: Please see Appendix A. □

TABLE III
ASYMPTOTIC SNR

	Passive RIS	Active RIS	Active/Passive RIS			Active/Active RIS	
			$N_1 = 3N/4$	$N_1 = N/2$	$N_1 = N/4$	$S = 2$	$S = 4$
SNR [dB]	$P_{\max} = 2$ W 39.08	$P_{\max} = 2$ W 78.97	$P_{\max} = 2$ W 77.72	$P_{\max} = 2$ W 75.96	$P_{\max} = 2$ W 72.95	$P_{\max} = 2$ W 77.21	$P_{\max} = 2$ W 74.99
	$P_{\max} = 3$ W 40.84	$P_{\max} = 3$ W 80.73	$P_{\max} = 3$ W 79.48	$P_{\max} = 3$ W 77.72	$P_{\max} = 3$ W 74.71	$P_{\max} = 3$ W 78.97	$P_{\max} = 3$ W 76.75
SNR for Large P_t [dB]	$P_{\max} = 2$ W N/A	$P_{\max} = 2$ W 81.98	$P_{\max} = 2$ W 27.04	$P_{\max} = 2$ W 33.06	$P_{\max} = 2$ W 36.58	$P_{\max} = 2$ W 78.97	$P_{\max} = 2$ W 75.96
	$P_{\max} = 3$ W N/A	$P_{\max} = 3$ W 83.74	$P_{\max} = 3$ W 28.81	$P_{\max} = 3$ W 34.82	$P_{\max} = 3$ W 38.35	$P_{\max} = 3$ W 80.73	$P_{\max} = 3$ W 77.72
SNR for Large P_r [dB]	$P_{\max} = 2$ W N/A	$P_{\max} = 2$ W 81.98	$P_{\max} = 2$ W 80.73	$P_{\max} = 2$ W 78.97	$P_{\max} = 2$ W 75.96	$P_{\max} = 2$ W 81.98	$P_{\max} = 2$ W 81.98
	$P_{\max} = 3$ W N/A	$P_{\max} = 3$ W 83.74	$P_{\max} = 3$ W 82.49	$P_{\max} = 3$ W 80.73	$P_{\max} = 3$ W 77.72	$P_{\max} = 3$ W 83.74	$P_{\max} = 3$ W 83.74

Remark 6: Given that $N_1 \triangleq aN$, $a \in (0,1)$, we note that $\gamma_{a/p}\left(N, P_{t,a/p}^{\max}, P_{r,1}^{\max}\right) \approx \gamma_a\left(aN, P_{t,a/p}^{\max}, P_{r,1}^{\max}\right) = a\gamma_a\left(N, P_{t,a/p}^{\max}, P_{r,1}^{\max}\right)$, i.e., the passive RS has negligible impact on the SNR and active RIS outperforms active/passive RIS by a factor of $1/a$ in the standard operation regime.

Remark 7: By letting $P_{r,1}^{\max} \to \infty$ in Eq. (15), the asymptotic SNR is upper-bounded by $\gamma_{a/p}^{\infty_r}\left(N, P_{t,a/p}^{\max}\right) \to \gamma_a^{\infty_r}\left(aN, P_{t,a/p}^{\max}\right) = a\gamma_a^{\infty_r}\left(N, P_{t,a/p}^{\max}\right)$, similar to the standard operation regime. For large values of the transmit power $P_{t,a/p}^{\max}$, on the other hand, given that $N_2 \triangleq (1-a)N$, we have $\gamma_{a/p}\left(N, P_{t,a/p}^{\max}, P_{r,1}^{\max}\right) \approx \gamma_p\left((1-a)N, P_{t,a/p}^{\max}\right) = (1-a)^2\gamma_p\left(N, P_{t,a/p}^{\max}\right)$, i.e., as we increase $P_{t,a/p}^{\max}$, active RS's impact is reduced and passive RIS outperforms active/passive RIS by a factor of $1/(1-a)^2$.

Remark 8: For large N, if $N_1 \gg N_2$, then $\gamma_{a/p}\left(N, P_{t,a/p}^{\max}, P_{r,1}^{\max}\right) = \gamma_a\left(N_1, P_{t,a/p}^{\max}, P_{r,1}^{\max}\right)$, while if $N_2 \gg N_1$,

$$\begin{aligned}
&\gamma_{a/p}\left(N, P_{t,a/p}^{\max}, P_{r,1}^{\max}\right) = \\
&= \gamma_p\left(N_2, P_{t,a/p}^{\max}\right) \frac{\left(P_{t,a/p}^{\max}\varrho_{g_1}^2 + \delta_1^2\right)\sigma^2}{\left(P_{r,1}^{\max}\delta_1^2\varrho_{f_1}^2 + P_{t,a/p}^{\max}\sigma^2\varrho_{g_1}^2 + \sigma^2\delta_1^2\right)} \\
&= \gamma_a\left(N_2, P_{t,a/p}^{\max}, P_{r,1}^{\max}\right) \frac{\left(P_{t,a/p}^{\max}\varrho_{g_1}^2 + \delta_1^2\right)N_2}{P_{r,1}^{\max}}. \qquad (16)
\end{aligned}$$

Thus, the active RS impacts SNR, even when $N_2 \gg N_1$.

Remark 9: In Cases 1, 2, and 3, where $a = a_1 = 3/4$, $a = a_2 = 1/2$, and $a = a_3 = 1/4$, the SNR loss, $10\log_{10}(a)$, compared to active RIS in both the standard and large reflect power regimes, where the active RIS nature dominates, is 1.25 dB, 3.01 dB, and 6.02 dB, respectively, as shown in Table III. Hence, the SNR loss when a is reduced from 3/4 to 1/2 and then from 1/2 to 1/4, $10\log_{10}(a_i) - 10\log_{10}(a_{i+1})$, $i = 1, 2$, is 1.76 dB and 3.01 dB, respectively. On the other hand, in Cases 3, 2, and 1, where $1-a = b_1 = 3/4$, $1-a = b_2 = 1/2$, and $1-a = b_3 = 1/4$, the SNR loss, $20\log_{10}(1-a)$, compared to passive RIS in the large transmit power regime, where the passive RIS nature dominates, is 2.5 dB, 6.02 dB, and 12.04 dB, respectively. Hence, the SNR loss when $1-a$ is reduced from 3/4 to 1/2 and then from 1/2 to 1/4, $20\log_{10}(b_i) - 20\log_{10}(b_{i+1})$, $i = 1, 2$, is 3.52 dB and 6.02 dB, respectively. Increasing $P_{\max}$ by 50% or the transition to the large reflect power regime result in an SNR gain of 1.76 dB or 3.01 dB, respectively, similar to active RIS.

Lemma 4 (Asymptotic SNR for active/active RIS): Letting $N_s \to \infty$, the asymptotic SNR for the active/active RIS case with equal REs allocation, i.e., $N_s = N/S$, and arbitrary number of RSs S is given by

$$\begin{aligned}
&\gamma_{a/a}\left(N, P_{t,a/a}^{\max}, P_{r,s}^{\max}\right) \to \\
&\sum_{s\in\mathcal{S}} \frac{N}{S} \frac{P_{r,s}^{\max}\pi^2\varrho_{f_s}^2\varrho_{g_s}^2\left(P_{t,a/a}^{\max}\varrho_{g_s}^2 + \delta_s^2\right)}{16\left[P_{r,s}^{\max}\delta_s^2\varrho_{f_s}^2 + \sigma^2\left(P_{t,a/a}^{\max}\varrho_{g_s}^2 + \delta_s^2\right)\right]\left(\varrho_{g_s}^2 + \delta_s^2\right)}. \qquad (17)
\end{aligned}$$

Proof: Please see Appendix B. □

Remark 10: Given that $P_{r,s}^{\max} = P_r^{\max}/S$, we note that

$$\begin{aligned}
&\gamma_{a/a}\left(N, P_{t,a/a}^{\max}, P_{r,s}^{\max}\right) \to \\
&\sum_{s\in\mathcal{S}} \gamma_a\left(\frac{N}{S}, P_{t,a/a}^{\max}, \frac{P_r^{\max}}{S}\right) \frac{\varrho_{g_s}^2 P_{t,a/a}^{\max} + \delta_s^2}{P_{t,a/a}^{\max}\left(\varrho_{g_s}^2 + \delta_s^2\right)} \\
&\approx S\gamma_a\left(\frac{N}{S}, P_{t,a/a}^{\max}, \frac{P_r^{\max}}{S}\right) = \gamma_a\left(N, P_{t,a/a}^{\max}, \frac{P_r^{\max}}{S}\right). \qquad (18)
\end{aligned}$$

Remark 11: By letting $P_{t,a/a}^{\max} \to \infty$ in Eq. (17), the asymptotic SNR of active/active RIS is upper-bounded by

$$\begin{aligned}
&\gamma_{a/a}^{\infty_t}\left(N, P_{r,s}^{\max}\right) \to \sum_{s\in\mathcal{S}} \frac{\gamma_a^{\infty_t}\left(\frac{N}{S}, \frac{P_r^{\max}}{S}\right)\varrho_{g_s}^2}{\varrho_{g_s}^2 + \delta_s^2} \\
&\approx S\gamma_a^{\infty_t}\left(\frac{N}{S}, \frac{P_r^{\max}}{S}\right) = \gamma_a^{\infty_t}\left(N, \frac{P_r^{\max}}{S}\right) \\
&= \frac{1}{S}\gamma_a^{\infty_t}\left(N, P_r^{\max}\right). \qquad (19)
\end{aligned}$$

Hence, active RIS outperforms active/active RIS by a factor of S. Likewise, by letting $P_{r,s}^{\max} \to \infty$ in Eq. (17), $\gamma_{a/a}^{\infty_r}\left(N, P_{t,a/a}^{\max}\right) \approx S\gamma_a^{\infty_r}\left(\frac{N}{S}, P_{t,a/a}^{\max}\right) = \gamma_a^{\infty_r}\left(N, P_{t,a/a}^{\max}\right)$.

Remark 12: As we see in Table III, active/active RIS with $S = S_1 = 2$ RSs outperforms its counterpart with $S = S_2 = 4$ RSs by 2.22 dB in the standard operation regime, irrespective

TABLE IV
REQUIRED NUMBER OF REs (IN MILLIONS)

	Active RIS	**Active/Passive RIS**			**Active/Active RIS**	
Passive RIS	2.5	$N_1 = 3N/4$ 1.90	$N_1 = N/2$ 1.33	$N_1 = N/4$ 0.72	$S = 2$ 1.66	$S = 4$ 1.00
Active/Passive RIS	40.00 ($N_1 = 3N/4$) 20.00 ($N_1 = N/2$) 13.33 ($N_1 = N/4$)					

of $P_{\max}$. This is due to the smaller reflect power budget per RS for larger number of RSs, as shown in Eq. (18). In the large transmit power regime, where the impact of the reflect power budget is pronounced, this SNR gain becomes $10\log_{10}(S_2) - 10\log_{10}(S_1) = 10\log 10(2) = 3.01$ dB, as seen in Eq. (19). On the other hand, in the large reflect power regime, the performance of these variants is identical, since the transmit power budget is the same in both cases, as seen in Remark 11. An increase of $P_{\max}$ by 50% results in an SNR gain of $10\log_{10}(1.5) = 1.76$ dB in all operation regimes. Active RIS outperforms active/active RIS by 1.76 dB ($S = 2$) or 3.98 dB ($S = 4$) in the standard operation regime and by 3.01 dB ($S = 2$) or 6.02 dB ($S = 4$) (i.e., by $10\log_{10}(S)$) in the large transmit power regime, irrespective of $P_{\max}$, while in the large reflect power regime, these hybrid RIS architectures achieve the same performance, regardless of the TPC budget or the number of RSs, as expected from Remark 11. Active/active RIS outperforms active/passive RIS Cases 1, 2, and 3 by 1.25 dB, 3.01 dB, and 6.02 dB, respectively, i.e., by $10\log_{10}(a)$, as expected from Remarks 7 and 11. It significantly outperforms also these active/passive RIS cases in the large transmit power regime, as expected. In the standard operation regime, it outperforms Case 3 by 4.26 dB ($S = 2$) or 2.04 dB ($S = 4$); it presents an SNR gain of 1.25 dB ($S = 2$) or an SNR loss of 0.97 dB ($S = 4$) compared to Case 2; and it presents an SNR loss of 0.51 dB ($S = 2$) or 2.73 dB ($S = 4$) compared to Case 1, irrespective of $P_{\max}$.

B. Impact of RIS Size

Next, we compare the SNR of these RIS designs with respect to the RIS size.

Lemma 5 (RIS size—passive vs. active RIS): For large N, passive RIS outperforms active RIS when

$$N \geq \frac{P_{t,a}^{\max}}{P_{t,p}^{\max}} \frac{P_r^{\max}\sigma^2}{P_r^{\max}\delta^2\varrho_f^2 + P_{t,a}^{\max}\sigma^2\varrho_g^2 + \sigma^2\delta^2} \triangleq N_{\min}. \quad (20)$$

Proof: The proof can be found in [20]. □

Remark 13: We notice in Table IV that passive RIS outperforms active RIS only when $N \geq N_{\min} = 2.5 \times 10^6$, regardless of $P_{\max}$. The deployment of such an extremely large number of REs is impractical in terms of hardware, channel estimation, and real-time RB.

Lemma 6 (RIS size—passive vs. active/passive RIS): For large N and arbitrary REs' allocation, i.e., $N_1 = aN$ and $N_2 = (1-a)N$, $a \in (0,1)$, such that $N_1 + N_2 = N$, passive RIS outperforms active/passive RIS when the number of REs satisfies Eq. (21) at the top of the next page.

Proof: Solve $\gamma_p \geq \gamma_{a/p}$ for N. □

Remark 14: As shown in Table IV, approximately $N \geq 1.90 \times 10^6$, $N \geq 1.33 \times 10^6$, and $N \geq 0.72 \times 10^6$ REs are required, for passive RIS to outperform active/passive RIS in Cases 1, 2, and 3, respectively, regardless of $P_{\max}$. Hence, fewer REs are required, compared to the active RIS case, and this figure is reduced as the number of active REs is decreased. These results agree with the SNRs in Table III. A simple, yet quite accurate, approximation, derived by Remark 6 and Eq. (20), is $N \geq aN_{\min}$. Then, for Cases 1, 2, and 3, where a equals $3/4$, $1/2$, and $1/4$, $N \geq 1.875 \times 10^6$, $N \geq 1.25 \times 10^6$, and $N \geq 0.625 \times 10^6$, respectively.

Lemma 7 (RIS size—passive vs. active/active RIS): For large N, an arbitrary number of RSs S, and $N_s = N/S$, passive RIS outperforms active/active RIS when the number of REs satisfies Eq. (22) at the top of the next page, where the approximation is derived by Remark 10 and Eq. (20).

Proof: Solve $\gamma_p \geq \gamma_{a/a}$ for N. □

Remark 15: We notice in Table IV that about $N \geq 1.66 \times 10^6$ or $N \geq 1 \times 10^6$ REs are required, regardless of $P_{\max}$, for passive RIS to outperform active/active RIS with $S = 2$ or $S = 4$ RSs, respectively. The reduction in the required number of REs is due to the negative impact on the SNR of the smaller reflect power in each RS for higher number of RSs. We note that more REs are required in the active/passive RIS Case 1 compared to the active/active RIS variants as well as in Case 2 compared to the variant with $S = 4$. These results are in agreement with the SNR values listed in Table III.

Lemma 8 (RIS size—active/passive vs. active RIS): For large N and arbitrary REs' allocation, i.e., $N_1 = aN$ and $N_2 = (1-a)N$, $a \in (0,1)$, such that $N_1 + N_2 = N$, active/passive RIS outperforms active RIS when the number of REs satisfies Eq. (23) at the top of the next page.

Proof: Solve $\gamma_{a/p} \geq \gamma_a$ for N. □

Remark 16: We note in Table IV that active/passive RIS Case 1, 2, and 3 outperforms active RIS when the total number of REs respectively satisfies $N \geq 40 \times 10^6$, $N \geq 20 \times 10^6$, and $N \geq 13.33 \times 10^6$, regardless of the value of $P_{\max}$. In other words, while, as shown in Table III, active/passive RIS substantially outperforms passive RIS, it needs a much larger number of REs than passive RIS to achieve the performance of active RIS. Although this result seems counter-intuitive at first glance, it is easily explained. Let's consider an active RIS with N_a REs, a passive RIS with N_p REs, and an active/passive RIS with N_1 active and N_2 passive REs, such that $N_1 + N_2 = N$. As we see in Remark 6, active/passive RIS behaves essentially as an active RIS with $N_1 < N_a$ REs; therefore, we cannot reach active RIS performance by increasing N_1. In practice, there is some SNR contribution from the passive RS, as seen in Eq. (15). Therefore, we will eventually reach the performance

$$N \geq \frac{a\left(P_{t,a/p}^{\max}\right)^2 P_{r,1}^{\max}\sigma^2\varrho_{f_1}^2\varrho_{g_1}^2}{\left(P_{r,1}^{\max}\delta_1^2\varrho_{f_1}^2 + P_{t,a/p}^{\max}\sigma^2\varrho_{g_1}^2 + \sigma^2\delta_1^2\right)P_{t,p}^{\max}P_{t,a/p}^{\max}\varrho_f^2\varrho_g^2 - (1-a)^2 P_{t,a/p}^{\max}\sigma^2\varrho_{f_2}^2\varrho_{g_2}^2\left(P_{t,a/p}^{\max}\varrho_{g_1}^2 + \delta_1^2\right)}. \tag{21}$$

$$N \geq \frac{\sigma^2}{SP_{t,p}^{\max}\varrho_f^2\varrho_g^2}\sum_{s\in\mathcal{S}}\frac{P_{r,s}^{\max}\varrho_{f_s}^2\varrho_{g_s}^2\left(P_{t,a/a}^{\max}\varrho_{g_s}^2 + \delta_s^2\right)}{\left[P_{r,s}\delta_s^2\varrho_{f_s}^2 + \sigma^2\left(P_{t,a/a}^{\max}\varrho_{g_s}^2 + \delta_s^2\right)\right]\left(\varrho_{g_s}^2 + \delta_s^2\right)} \approx \frac{P_{t,a/a}^{\max}\sigma^2}{SP_{t,p}^{\max}}\sum_{s\in\mathcal{S}}\frac{P_r^{\max}}{P_r^{\max}\delta_s^2\varrho_{f_s}^2 + SP_{t,a/a}^{\max}\sigma^2\varrho_{g_s}^2 + S\sigma^2\delta_s^2}. \tag{22}$$

$$N \geq \frac{\left[P_{t,a}^{\max}P_r^{\max}\varrho_f^2\varrho_g^2\left(P_{r,1}^{\max}\delta_1^2\varrho_{f_1}^2 + P_{t,a/p}^{\max}\sigma^2\varrho_{g_1}^2 + \sigma^2\delta_1^2\right) - aP_{t,a/p}^{\max}P_{r,1}^{\max}\varrho_{f_1}^2\varrho_{g_1}^2\left(P_r^{\max}\delta^2\varrho_f^2 + P_{t,a}^{\max}\sigma^2\varrho_g^2 + \sigma^2\delta^2\right)\right]P_{t,a/p}^{\max}}{(1-a)^2 P_{t,a/p}^{\max}\varrho_{f_2}^2\varrho_{g_2}^2\left(P_{t,a/p}^{\max}\varrho_{g_1}^2 + \delta_1^2\right)\left(P_r^{\max}\delta^2\varrho_f^2 + P_{t,a}^{\max}\sigma^2\varrho_g^2 + \sigma^2\delta^2\right)}. \tag{23}$$

of active RIS even with $N_1 > N_2$, but it will require a very large total number of REs N, as we see in Table IV, since the contribution of the passive RS is very small. As we keep increasing the number of passive REs in the active/passive RIS, correspondingly reducing at the same time the number of active REs, the impact of the passive RS increases as well, until the point where we heavily favor passive REs over active ones, i.e., $N_2 \gg N_1$, which is described by Eq. (16). This explains why a smaller total number of REs is needed when there are more passive than active REs. Nevertheless, since $N_2 < N_p$, and there is also a negative impact on the SNR by amplification noise as shown by the nominator of Eq. (16), a greater number of REs than in passive RIS case is needed.

Lemma 9 (RIS size—active/active vs. active RIS): For large N and N_a, since $P_{t,a/a}^{\max} = P_{t,a}^{\max}$, active/active RIS with N REs and S RSs outperforms active RIS with N_a REs when

$$N \geq N_a\frac{P_r^{\max}\delta^2\varrho_f^2 + SP_{t,a}^{\max}\sigma^2\varrho_g^2 + S\sigma^2\delta^2}{P_r^{\max}\delta^2\varrho_f^2 + P_{t,a}^{\max}\sigma^2\varrho_g^2 + \sigma^2\delta^2}. \tag{24}$$

Proof: Set $\gamma_{a/a} \geq \gamma_a$, i.e., $\gamma_a\left(N, P_{t,a}^{\max}, P_r^{\max}/S\right) \geq \gamma_a\left(N_a, P_{t,a}^{\max}, P_r^{\max}\right)$, and solve for N. □

Remark 17: From Lemma 9, it becomes apparent that more REs are required, for higher number of RSs. Specifically, assuming $N_a = 256$, $N \geq 384 = 1.5N_a$ for $S = 2$ and $N \geq 640 = 2.5N_a$ for $S = 4$, respectively.

IV. Problem Formulation and Solutions

A. Hybrid Active/Passive RIS

In the hybrid active/passive RIS case, the optimization problem of interest is mathematically formulated as follows:

$$\text{(P1)}: \max_{\mathbf{w},\{\boldsymbol{\phi}_s\}} \eta = \frac{R}{P} = \frac{\sum_{k\in\mathcal{K}}\log_2(1+\gamma_k)}{\widetilde{P} + P_1 + N_2P_{\text{PS}}} \tag{25a}$$

$$\text{s.t.} \quad \text{C1: } P_{\text{BS}} = \xi^{-1}\sum_{k\in\mathcal{K}}\|\mathbf{w}_k\|^2 + W_{\text{BS}} \leq P_{\text{BS}}^{\max}, \tag{25b}$$

$$\text{C2: } P_1 = \zeta_1^{-1}\left(\sum_{k\in\mathcal{K}}\|\boldsymbol{\Phi}_1\mathbf{G}_1\mathbf{w}_k\|^2 + \delta_1^2\|\boldsymbol{\Phi}_1\|_F^2\right) + W_{r,1} \leq P_1^{\max}, \tag{25c}$$

$$\text{C3: } |[\boldsymbol{\phi}_2]_n| = 1, \ \forall n \in \mathcal{N}_2, \tag{25d}$$

where we have respectively defined $\mathbf{w} \in \mathbb{C}^{KM}$ and $\boldsymbol{\phi}_s \in \mathbb{C}^{N_s}$ as $\mathbf{w} \triangleq \left[\mathbf{w}_1^T, \ldots, \mathbf{w}_K^T\right]^T$ and $\boldsymbol{\phi}_s \triangleq \text{Diag}\left(\boldsymbol{\Phi}_s^*\right)$, γ_k is given by Eq. (7), and $W_{r,1}$ is given by either Eq. (5a) or Eq. (5b).

(P1) is a challenging non-convex optimization problem, due to the fractional form of the objective function (OF), the intrinsic coupling of the decision variables in the OF and the constraints, and the unit modulus constraints (UMC) C3.

1) Fractional Programming: Using Dinkelbach's algorithm, we convert the OF to $f(\mathbf{w},\boldsymbol{\phi}) = R - \eta P$ [6], where $\boldsymbol{\phi} \triangleq \left[\boldsymbol{\phi}_1^T, \boldsymbol{\phi}_2^T\right]^T$. By applying the Lagrangian dual transform and the quadratic transform [25], we recast (P1) as:

$$\text{(P2)}: \max_{\mathbf{w},\boldsymbol{\phi},\boldsymbol{\mu},\boldsymbol{\nu}} g(\mathbf{w},\boldsymbol{\phi},\boldsymbol{\mu},\boldsymbol{\nu}) \ \text{ s.t. C1–C3}, \tag{26}$$

where $\boldsymbol{\mu} \in \mathbb{C}^K$ and $\boldsymbol{\nu} \in \mathbb{C}^K$ are auxiliary variables and

$$\begin{aligned} g(\mathbf{w},\boldsymbol{\phi},\boldsymbol{\mu},\boldsymbol{\nu}) &= -\eta P \\ &+ \sum_{k\in\mathcal{K}}\Big[\ln(1+\mu_k) - \mu_k + 2\sqrt{1+\mu_k}\,\text{Re}\left\{\nu_k^*\mathbf{h}_k^\dagger\mathbf{w}_k\right\} \\ &- |\nu_k|^2\left(\sum_{i\in\mathcal{K}}\left|\mathbf{h}_k^\dagger\mathbf{w}_i\right|^2 + \left\|\mathbf{f}_{k,1}^\dagger\boldsymbol{\Phi}_1\right\|^2\delta_1^2 + \sigma_k^2\right)\Big]. \end{aligned} \tag{27}$$

Next, we alternately optimize each variable with the others being fixed in each iteration until we reach convergence to a locally optimal solution.

2) Optimal Auxiliary Variables: Setting $\partial g/\partial\mu_k = 0$ and $\partial g/\partial\nu_k = 0$ with fixed $(\mathbf{w},\boldsymbol{\phi},\boldsymbol{\nu})$ and $(\mathbf{w},\boldsymbol{\phi},\boldsymbol{\mu})$, respectively, and defining $\rho_k \triangleq \text{Re}\left\{\nu_k^*\mathbf{h}_k^\dagger\mathbf{w}_k\right\}$, we obtain:

$$\mu_k^\star = \frac{\rho_k}{2}\left(\rho_k + \sqrt{\rho_k^2+4}\right), \tag{28a}$$

$$\nu_k^\star = \frac{\sqrt{1+\mu_k}\mathbf{h}_k^\dagger\mathbf{w}_k}{\sum_{i\in\mathcal{K}}\left|\mathbf{h}_k^\dagger\mathbf{w}_i\right|^2 + \left\|\mathbf{f}_{k,1}^\dagger\boldsymbol{\Phi}_1\right\|^2\delta_1^2 + \sigma_k^2}. \tag{28b}$$

3) Optimal Transmit Precoding: We note in Eqs. (25b) and (25c) that the TSP budget of the BS and RS1 equal

$$\widetilde{P}_{\text{BS}}^{\max} = \xi\left(P_{\text{BS}}^{\max} - W_{\text{BS}}\right), \tag{29a}$$

$$\widetilde{P}_1^{\max} = \zeta_1\left(P_1^{\max} - W_{r,1}\right). \tag{29b}$$

Let us define $\mathbf{H}_k \in \mathbb{C}^{M\times M}$ as $\mathbf{H}_k \triangleq \mathbf{h}_k\mathbf{h}_k^\dagger$ and $\mathbf{u}_k \in \mathbb{C}^M$, $\mathbf{u} \in \mathbb{C}^{KM}$, $\mathbf{S} \in \mathbb{C}^{KM\times KM}$, and $\mathbf{T} \in \mathbb{C}^{KM\times KM}$ as

$$\mathbf{u}_k \triangleq 2\sqrt{1+\mu_k}\nu_k\mathbf{h}_k,\ \mathbf{u} \triangleq \left[\mathbf{u}_1^T,\ldots,\mathbf{u}_K^T\right]^T, \tag{30a}$$

$$\mathbf{S} \triangleq \mathbf{I}_K \otimes \left(\eta\xi^{-1}\mathbf{I}_M + \eta\zeta_1^{-1}\mathbf{G}_1^\dagger\mathbf{\Phi}_1^\dagger\mathbf{\Phi}_1\mathbf{G}_1 + \sum_{k\in\mathcal{K}}|\nu_k|^2\mathbf{H}_k\right), \tag{30b}$$

$$\mathbf{T} \triangleq \mathbf{I}_K \otimes \left(\mathbf{G}_1^\dagger\mathbf{\Phi}_1^\dagger\mathbf{\Phi}_1\mathbf{G}_1\right). \tag{30c}$$

Hence, with fixed $(\boldsymbol{\phi},\boldsymbol{\mu},\boldsymbol{\nu})$, the TP optimization sub-problem can be formulated as follows:

$$\text{(P3)}: \max_{\mathbf{w}} \operatorname{Re}\left\{\mathbf{u}^\dagger\mathbf{w}\right\} - \mathbf{w}^\dagger\mathbf{S}\mathbf{w} \tag{31a}$$

$$\text{s.t.}\quad \text{C1: } \mathbf{w}^\dagger\mathbf{w} \le \widetilde{P}_{\text{BS}}^{\max}, \tag{31b}$$

$$\text{C2: } \mathbf{w}^\dagger\mathbf{T}\mathbf{w} \le \widetilde{P}_1^{\max} - \delta_1^2\left\|\mathbf{\Phi}_1\right\|_F^2. \tag{31c}$$

(P3) is a standard convex Quadratically Constrained Quadratic Program (QCQP), which can be solved by using the Lagrange multipliers method to obtain [20]

$$\mathbf{w}^\star = \frac{1}{2}(\mathbf{S} + \lambda_1\mathbf{I}_{KM} + \lambda_2\mathbf{T})^{-1}\mathbf{u}, \tag{32}$$

where the Lagrange multipliers corresponding to the constraints C1 and C2, λ_1 and λ_2, are optimized via grid search.

4) Optimal RIS Beamforming: Let $\alpha_{k,i} \triangleq \mathbf{g}_k^\dagger\mathbf{w}_i$. We define $\boldsymbol{\beta}_{s,i} \in \mathbb{C}^N$ as $\boldsymbol{\beta}_{s,i} \triangleq \mathbf{G}_s\mathbf{w}_i$. Then, $\mathbf{h}_k^\dagger\mathbf{w}_i \triangleq \alpha_{k,i} + \mathbf{f}_{k,s}^\dagger\operatorname{diag}(\boldsymbol{\beta}_{s,i})\boldsymbol{\phi}_s$. We also define $\boldsymbol{\upsilon}_s \in \mathbb{C}^{N_s}$, $\mathbf{Q}_s \in \mathbb{C}^{N_s\times N_s}$, $\mathbf{Q}_s \succeq \mathbf{0}$, and $\mathbf{R} \in \mathbb{C}^{N_1\times N_1}$ as

$$\boldsymbol{\upsilon}_s \triangleq \sum_{k\in\mathcal{K}}\operatorname{diag}\left(\mathbf{f}_{k,s}^\dagger\right)\left(2\sqrt{1+\mu_k}\nu_k^*\boldsymbol{\beta}_{s,k} - |\nu_k|^2\sum_{i\in\mathcal{K}}\alpha_{k,i}^*\boldsymbol{\beta}_{s,i}\right), \tag{33a}$$

$$\mathbf{Q}_1 \triangleq \sum_{k\in\mathcal{K}}\left(|\nu_k|^2\delta_1^2\operatorname{diag}\left(\mathbf{f}_{k,1}\odot\mathbf{f}_{k,1}^*\right) + \eta\zeta_1\operatorname{diag}\left(\boldsymbol{\beta}_{1,k}\odot\boldsymbol{\beta}_{1,k}^*\right)\right) + \sum_{k\in\mathcal{K}}|\nu_k|^2\sum_{i\in\mathcal{K}}\operatorname{diag}\left(\boldsymbol{\beta}_{1,i}^*\right)\mathbf{f}_{k,1}\mathbf{f}_{k,1}^\dagger\operatorname{diag}\left(\boldsymbol{\beta}_{1,i}\right) + \eta\zeta_1\delta_1^2\mathbf{I}_{N_1}, \tag{33b}$$

$$\mathbf{Q}_2 \triangleq \sum_{k\in\mathcal{K}}|\nu_k|^2\sum_{i\in\mathcal{K}}\operatorname{diag}\left(\boldsymbol{\beta}_{2,i}^*\right)\mathbf{f}_{k,2}\mathbf{f}_{k,2}^\dagger\operatorname{diag}\left(\boldsymbol{\beta}_{2,i}\right), \tag{33c}$$

$$\mathbf{R} \triangleq \sum_{k\in\mathcal{K}}\operatorname{diag}\left(\boldsymbol{\beta}_{1,k}\odot\boldsymbol{\beta}_{1,k}^*\right) + \delta_1^2\mathbf{I}_{N_1}. \tag{33d}$$

Hence, by fixing $(\mathbf{w},\boldsymbol{\phi}_2,\boldsymbol{\mu},\boldsymbol{\nu})$ and dropping the respective constant terms from the OF, we obtain the following sub-problem for optimizing $\boldsymbol{\phi}_1$:

$$\text{(P4-A)}: \max_{\boldsymbol{\phi}_1}\operatorname{Re}\left\{\boldsymbol{\phi}_1^\dagger\boldsymbol{\upsilon}_1\right\} - \boldsymbol{\phi}_1^\dagger\mathbf{Q}_1\boldsymbol{\phi}_1 \text{ s.t. C2: } \boldsymbol{\phi}_1^\dagger\mathbf{R}\boldsymbol{\phi}_1 \le \widetilde{P}_1^{\max}. \tag{34}$$

We use the Lagrange multipliers method to tackle this standard QCQP and obtain a closed-form expression of $\boldsymbol{\phi}_1^\star$:

$$\boldsymbol{\phi}_1^\star = \frac{1}{2}\left(\mathbf{Q}_1 + \varpi\mathbf{R}\right)^{-1}\boldsymbol{\upsilon}_1, \tag{35}$$

where the Lagrange multiplier associated with C2, ϖ, is optimized via binary search. Then, $\mathbf{\Theta}_1^\star = \operatorname{diag}\left(e^{j\arg((\boldsymbol{\phi}_1^\star)^*)}\right)$ and $[\mathbf{A}_1^\star]_{n,n} = |[\boldsymbol{\phi}_1^\star]_n|$ or $\boldsymbol{\alpha}_1^\star = \mathbf{\Gamma}_1^+\operatorname{diag}\left(e^{-j\arg((\boldsymbol{\phi}_1^\star)^*)}\right)(\boldsymbol{\phi}_1^\star)^*$ when RS1 adopts the FC- or SC-active design, respectively [6].

With fixed $(\mathbf{w},\boldsymbol{\phi}_1,\boldsymbol{\mu},\boldsymbol{\nu})$, we form the minimization sub-problem:

$$\text{(P4-B)}: \min_{\boldsymbol{\phi}_2} h(\boldsymbol{\phi}_2) = \boldsymbol{\phi}_2^\dagger\mathbf{Q}_2\boldsymbol{\phi}_2 - \operatorname{Re}\left\{\boldsymbol{\phi}_2^\dagger\boldsymbol{\upsilon}_2\right\} \text{ s.t. C3.} \tag{36}$$

We apply the MM method to handle the UMCs C3. Specifically, for any given solution $\boldsymbol{\phi}_2^t$ at the t-th iteration of the MM algorithm and any feasible $\boldsymbol{\phi}_2$, we have [26]

$$\boldsymbol{\phi}_2^\dagger\mathbf{Q}_2\boldsymbol{\phi}_2 \le \boldsymbol{\phi}_2^\dagger\mathbf{X}\boldsymbol{\phi}_2 - 2\operatorname{Re}\left\{\boldsymbol{\phi}_2^\dagger\left(\mathbf{X}-\mathbf{Q}_2\right)\boldsymbol{\phi}_2^t\right\} + \left(\boldsymbol{\phi}_2^t\right)^\dagger\left(\mathbf{X}-\mathbf{Q}_2\right)\boldsymbol{\phi}_2^t \triangleq y\left(\boldsymbol{\phi}_2|\boldsymbol{\phi}_2^t\right), \tag{37}$$

where $\mathbf{X} = \lambda_{\max}\mathbf{I}_{N_2}$, $\lambda_{\max}$ denotes the maximum eigenvalue of $\mathbf{Q}_2$, and $\mathbf{X} \succeq \mathbf{Q}_2$, $\mathbf{X} \in \mathbb{R}_+^{N_2\times N_2}$. We replace the OF in (P4-B) by a surrogate OF, $z\left(\boldsymbol{\phi}_2|\boldsymbol{\phi}_2^t\right) \triangleq y\left(\boldsymbol{\phi}_2|\boldsymbol{\phi}_2^t\right) - \operatorname{Re}\left\{\boldsymbol{\phi}_2^\dagger\boldsymbol{\upsilon}_2\right\}$. The new OF represents an upper bound of the original one and coincides with it at point $\boldsymbol{\phi}_2^t$. By removing the constant terms in this new OF, such as $\boldsymbol{\phi}_2^\dagger\mathbf{X}\boldsymbol{\phi} = N_2\lambda_{\max}$, we obtain:

$$\text{(P4-C)}: \max_{\boldsymbol{\phi}_2}\ \operatorname{Re}\left\{\boldsymbol{\phi}_2^\dagger\mathbf{q}^t\right\} \text{ s.t. C3,} \tag{38}$$

where $\mathbf{q}^t \in \mathbb{C}^{N_2}$ is defined as $\mathbf{q}^t \triangleq \left(\mathbf{X}-\mathbf{Q}_2\right)\boldsymbol{\phi}_2^t + \boldsymbol{\upsilon}_2$ [26]. The optimal solution of problem (P4-C) is given by [26]

$$\boldsymbol{\phi}_2^{t+1} = e^{j\arg\left(\mathbf{q}^t\right)}. \tag{39}$$

B. Hybrid Active RIS

In the hybrid active RIS case, the optimization problem of interest is formulated as follows:

$$\text{(P5)}: \max_{\mathbf{w},\{\boldsymbol{\phi}_s\}} \eta = \frac{R}{P} = \frac{\sum_{k\in\mathcal{K}}\log_2\left(1+\gamma_k\right)}{\widetilde{P} + \sum_{s\in\mathcal{S}}P_s} \tag{40a}$$

$$\text{s.t.}\quad \text{C5: } P_{\text{BS}} = \xi^{-1}\sum_{k\in\mathcal{K}}\left\|\mathbf{w}_k\right\|^2 + W_{\text{BS}} \le P_{\text{BS}}^{\max}, \tag{40b}$$

$$\text{C6: } P_s = \zeta_s^{-1}\left(\sum_{k\in\mathcal{K}}\left\|\mathbf{\Phi}_s\mathbf{G}_s\mathbf{w}_k\right\|^2 + \delta_s^2\left\|\mathbf{\Phi}_s\right\|_F^2\right) + W_{r,s} \le P_s^{\max}, \forall s\in\mathcal{S}, \tag{40c}$$

where γ_k and $W_{r,2}$ are given by Eqs. (9) and (5b), respectively, whereas $W_{r,1}$ is given by either Eq. (5a) or Eq. (5b).

1) Fractional Programming: By using Dinkelbach's algorithm along with the Lagrangian dual and quadratic transforms [25], we equivalently recast (P5) as:

$$\text{(P6)}: \max_{\mathbf{w},\boldsymbol{\phi},\boldsymbol{\mu}',\boldsymbol{\nu}'} g'\left(\mathbf{w},\boldsymbol{\phi},\boldsymbol{\mu}',\boldsymbol{\nu}'\right) \text{ s.t. C5, C6,} \tag{41}$$

where $\boldsymbol{\mu}' \in \mathbb{C}^K$ and $\boldsymbol{\nu}' \in \mathbb{C}^K$ are auxiliary variables and

$$g'\left(\mathbf{w},\boldsymbol{\phi},\boldsymbol{\mu}',\boldsymbol{\nu}'\right) = -\eta P + \sum_{k\in\mathcal{K}}\left[\ln\left(1+\mu_k'\right) - \mu_k' + 2\sqrt{1+\mu_k'}\operatorname{Re}\left\{\left(\nu_k'\right)^*\mathbf{h}_k^\dagger\mathbf{w}_k\right\} - |\nu_k'|^2\left(\sum_{i\in\mathcal{K}}\left|\mathbf{h}_k^\dagger\mathbf{w}_i\right|^2 + \sum_{s\in\mathcal{S}}\left\|\mathbf{f}_{k,s}^\dagger\mathbf{\Phi}_s\right\|^2\delta_s^2 + \sigma_k^2\right)\right]. \tag{42}$$

Next, we develop a BCA algorithm to alternately optimize the auxiliary and decision variables.

2) Optimal Auxiliary Variables: Setting $\partial g'/\partial \mu'_k = 0$ and $\partial g'/\partial \nu'_k = 0$ with fixed $(\mathbf{w}, \boldsymbol{\phi}, \boldsymbol{\nu}')$ and $(\mathbf{w}, \boldsymbol{\phi}, \boldsymbol{\mu}')$, and defining $\rho'_k \triangleq \mathrm{Re}\left\{(\nu'_k)^* \mathbf{h}_k^\dagger \mathbf{w}_k\right\}$, we obtain

$$\mu_k'^{,\star} = \frac{\rho'_k}{2}\left(\rho'_k + \sqrt{(\rho'_k)^2 + 4}\right), \tag{43a}$$

$$\nu_k'^{,\star} = \frac{\sqrt{1+\mu'_k}\mathbf{h}_k^\dagger \mathbf{w}_k}{\sum\limits_{i\in\mathcal{K}} \left|\mathbf{h}_k^\dagger \mathbf{w}_i\right|^2 + \sum\limits_{s\in\mathcal{S}} \left\|\mathbf{f}_{k,s}^\dagger \boldsymbol{\Phi}_s\right\|^2 \delta_s^2 + \sigma_k^2}. \tag{43b}$$

3) Optimal Transmit Precoding: From Eq. (40c),

$$\widetilde{P}_2^{\max} = \zeta_2 \left(P_2^{\max} - W_{r,2}\right). \tag{44}$$

We also set $\mathbf{T}_1 = \mathbf{T}$ and respectively define $\mathbf{S}' \in \mathbb{C}^{KM\times KM}$ and $\mathbf{T}_2 \in \mathbb{C}^{KM\times KM}$ as

$$\mathbf{S}' \triangleq \mathbf{I}_K \otimes \left(\eta\xi^{-1}\mathbf{I}_M + \sum_{s\in\mathcal{S}} \eta\zeta_s^{-1}\mathbf{G}_s^\dagger \boldsymbol{\Phi}_s^\dagger \boldsymbol{\Phi}_s \mathbf{G}_s + \sum_{k\in\mathcal{K}} |\nu'_k|^2 \mathbf{h}_k \mathbf{h}_k^\dagger\right), \tag{45a}$$

$$\mathbf{T}_2 \triangleq \mathbf{I}_K \otimes \left(\mathbf{G}_2^\dagger \boldsymbol{\Phi}_2^\dagger \boldsymbol{\Phi}_2 \mathbf{G}_2\right). \tag{45b}$$

Hence, with fixed $(\boldsymbol{\phi}, \boldsymbol{\mu}', \boldsymbol{\nu}')$, the TP optimization sub-problem can be formulated as follows:

$$\text{(P7):} \max_{\mathbf{w}} \mathrm{Re}\left\{\mathbf{u}^\dagger \mathbf{w}\right\} - \mathbf{w}^\dagger \mathbf{S}' \mathbf{w} \tag{46a}$$

$$\text{s.t.} \quad \text{C5: } \mathbf{w}^\dagger \mathbf{w} \le \widetilde{P}_{\mathrm{BS}}^{\max}, \tag{46b}$$

$$\text{C6: } \mathbf{w}^\dagger \mathbf{T}_s \mathbf{w} \le \widetilde{P}_s^{\max} - \delta_s^2 \left\|\boldsymbol{\Phi}_s\right\|_F^2, \ \forall s \in \mathcal{S}. \tag{46c}$$

(P7) is a standard convex QCQP which can be solved by using the Lagrange multipliers method to obtain:

$$\mathbf{w}^\star = \frac{1}{2}(\mathbf{S}' + \lambda' \mathbf{I}_{KM} + \sum_{s\in\mathcal{S}} \psi_s \mathbf{T}_s)^{-1}\mathbf{u}, \tag{47}$$

where λ' and ψ_s represent the Lagrange multipliers that are associated with constraints C5 and C6, respectively, and are optimized via grid search.

4) Optimal RIS Beamforming: Let us define $\mathbf{Q}'_s \in \mathbb{C}^{N_s\times N_s}$ and $\mathbf{R}_s \in \mathbb{C}^{N_s\times N_s}$ as

$$\mathbf{Q}'_s \triangleq \sum_{k\in\mathcal{K}} \Big(|\nu'_k|^2 \delta_s^2 \,\mathrm{diag}\left(\mathbf{f}_{k,s} \odot \mathbf{f}_{k,s}^*\right) + \eta\zeta_s \,\mathrm{diag}\left(\boldsymbol{\beta}_{s,k} \odot \boldsymbol{\beta}_{s,k}^*\right)\Big) + \sum_{k\in\mathcal{K}} |\nu'_k|^2 \sum_{i\in\mathcal{K}} \mathrm{diag}\left(\boldsymbol{\beta}_{s,i}^*\right) \mathbf{f}_{k,s}\mathbf{f}_{k,s}^\dagger \,\mathrm{diag}\left(\boldsymbol{\beta}_{s,i}\right) + \eta\zeta_s\delta_s^2 \mathbf{I}_{N_s}, \tag{48a}$$

$$\mathbf{R}_s \triangleq \sum_{k\in\mathcal{K}} \mathrm{diag}\left(\boldsymbol{\beta}_{s,k} \odot \boldsymbol{\beta}_{s,k}^*\right) + \delta_s^2 \mathbf{I}_{N_s}. \tag{48b}$$

Hence, with fixed $(\mathbf{w}, \boldsymbol{\mu}', \boldsymbol{\nu}')$, we can formulate the RB optimization sub-problem as follows:

$$\text{(P8):} \max_{\boldsymbol{\phi}} \sum_{s\in\mathcal{S}} \left(\mathrm{Re}\left\{\boldsymbol{\phi}_s^\dagger \boldsymbol{\upsilon}_s\right\} - \boldsymbol{\phi}_s^\dagger \mathbf{Q}'_s \boldsymbol{\phi}_s\right) \tag{49a}$$

$$\text{s.t.} \quad \text{C6: } \boldsymbol{\phi}_s^\dagger \mathbf{R}_s \boldsymbol{\phi}_s \le \widetilde{P}_s^{\max}. \tag{49b}$$

Fixing $(\mathbf{w}, \boldsymbol{\phi}_{s'}, \boldsymbol{\mu}, \boldsymbol{\nu})$ and solving for $\boldsymbol{\phi}_s$, $s, s' \in \mathcal{S}$, $s' \neq s$, we formulate respective standard convex QCQPs. By using the Lagrange multipliers method, we obtain:

$$\boldsymbol{\phi}_s^\star = \frac{1}{2}\left(\mathbf{Q}'_s + \varpi_s \mathbf{R}_s\right)^{-1} \boldsymbol{\upsilon}_s, \tag{50}$$

where ϖ_s represents the Lagrange multiplier associated with the constraints C6 with fixed $s = 1$ or $s = 2$ in each case, respectively, and is optimized via binary search.

C. Complexity Analysis

The complexity of solving a standard convex QCQP having m variables and n constraints with an accuracy tolerance ε is given by $\mathcal{O}\left(\log_2(1/\varepsilon)\sqrt{m+n}(1+m)m^3\right)$ [20]. In (P3) and (P7), $m = MK$ and $n = 2$ or $n = 3$, respectively, while in (P4-A) and (P8-A), $m = N_1$ and $n = 1$. Likewise, in (P8-B), $m = N_2$ and $n = 1$. The combined complexity of (P3) and (P4-A) is given by $\mathcal{C}_1 = \mathcal{O}\left(\log_2(1/\varepsilon)\left(M^{4.5}K^{4.5} + N_1^{4.5}\right)\right)$. The complexity of the MM algorithm is dominated by the calculation of $\lambda_{\max}$ and $\mathbf{q}^t$ and is given by $\mathcal{C}_2 = \mathcal{O}\left(N_2^3 + I_{MM}N_2^2\right)$, where I_{MM} denotes the number of iterations required for converge [26]. The complexity of updating the auxiliary variables is dominated by the computation of complex inner products and equals $\mathcal{O}\left(KM\right)$ for $\boldsymbol{\mu}$ and $\boldsymbol{\mu}'$, $\mathcal{O}\left(K^2M + KN_1\right)$ for $\boldsymbol{\nu}$, and $\mathcal{O}\left(K^2M + KN\right)$ for $\boldsymbol{\nu}'$. Therefore, the overall complexity of the developed BCA algorithm for the active/passive and active/active RIS cases is respectively given by $\mathcal{O}\left(I_0 \max\left\{\mathcal{C}_1, \mathcal{C}_2\right\}\right)$ and $\mathcal{O}\left(\log_2(1/\varepsilon) I'_0\left(M^{4.5}K^{4.5} + N_1^{4.5} + N_2^{4.5}\right)\right)$, where I_0, I'_0 denote the number of iterations required for convergence.

V. Numerical Evaluations

Next, we validate the analytical results of Sec. III and comparatively evaluate the EE and SR of the proposed joint TB/RB designs against benchmarks via numerical simulations. We assume in the latter $N = 32$, $M = 4$, $K = 2$, $W_{\mathrm{BS}} = 6$ dBW, $W_{\mathrm{UE}} = W_{\mathrm{PS}} = W_{\mathrm{DC}} = 10$ dBm, $P_{\mathrm{BS}}^{\max} = P_s^{\max} = 9$ dBW, $\xi = \zeta_s = 0.909$, and $\sigma_k^2 = \sigma^2 = -80$ dBm, and $\delta_s^2 = \delta^2 = -80$ dBm, $\forall s \in \mathcal{S}$, $\forall k \in \mathcal{K}$. We consider Rician fading for all channels with Rician factor $\kappa = 5$ dB and path loss exponent $\alpha_{\mathrm{PL}} = 2.2$ [20]. The BS and RIS coordinates are $(0\mathrm{m},\ -20\mathrm{m},\ 0\mathrm{m})$ and $(100\mathrm{m},\ 5\mathrm{m},\ 0\mathrm{m})$, respectively.

A. Validation of Analytical Results

Fig. 3(a) plots the asymptotic SNR of the considered RIS architectures as the number of REs varies from 0.5×10^6 up to 3×10^6. This plot validates the results of Table IV, regarding the number of REs required, for passive RIS to outperform these designs. Furthermore, we note that active/passive RIS with $N/4$ active REs reaches the SNR of active/active RIS with 4 RSs when $N = 2.3\times10^6$ and starts to outperform it when $N = 2.9\times10^6$. In Fig. 3(b), the number of REs varies from 10×10^6 up to 50×10^6. We notice that passive RIS outperforms active RIS, as expected. This plot also validates the results of Table IV, regarding the number of REs required, for active/passive RIS Cases 1–3 to outperform active RIS. In Fig. 3(c), we validate that active/active RIS with $S = 2$ or $S = 4$ REs requires $1.5N$ or $2.5N$ REs, respectively, to reach the performance of an active RIS with N REs.

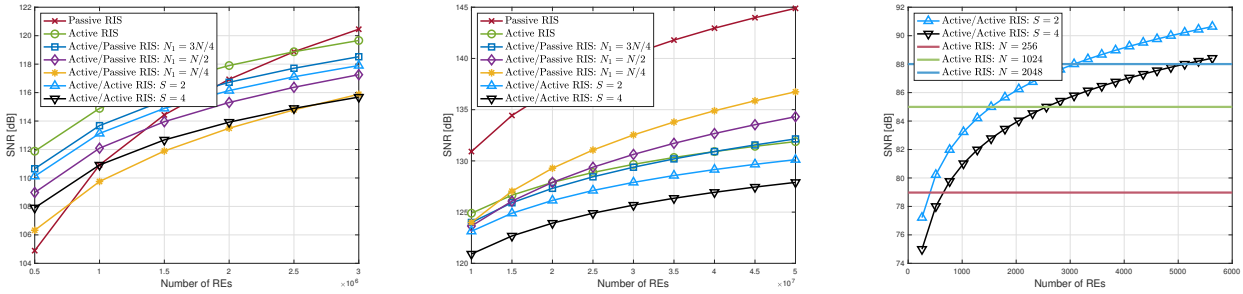

(a) N ranges from 0.5×10^6 up to 3×10^6. (b) N ranges from 10×10^6 up to 50×10^6. (c) N ranges from 256 up to 5636.

Fig. 3. Asymptotic SNR for the considered RIS architectures as the number of REs varies.

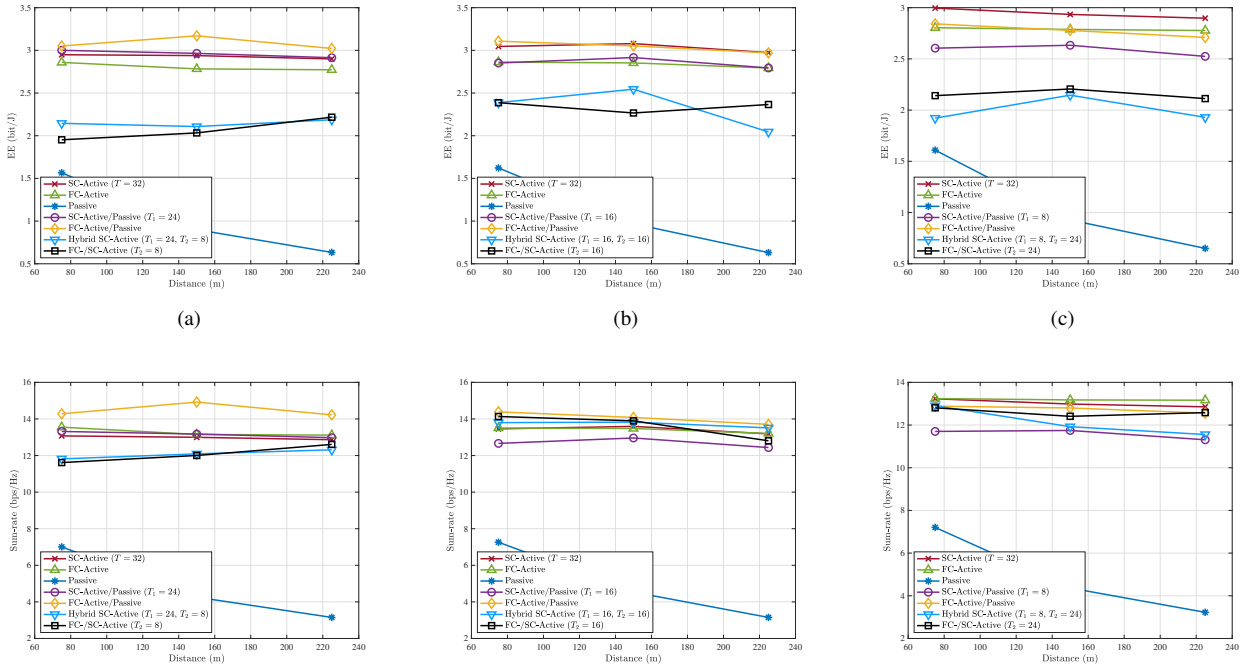

(a) (b) (c)

(d) (e) (f)

Fig. 4. EE (top) and SR (bottom) vs. user position for $\{N_1, N_2\} = \{\{24, 8\}, \{16, 16\}, \{8, 24\}\}$ ({left},{center},{right}) and $L = L_s = 1$, $\forall s$.

B. Optimization Results

In Fig. 4, the users are randomly located in a sphere with radius of 5 m centered at $(L, 0, 0)$, $L = 25 : 25 : 300$. We plot the performance of the different RIS types vs. the distance of the user cluster from the BS for various RIS configurations, assuming that the SC-active RIS and any such RS is equipped with a single reflect-type PA. Passive RIS achieves much lower EE and SR than all other RIS variants and its performance deteriorates quickly with the distance, due to the product path loss which greatly reduces the SR. Starting from the hybrid RIS configuration with the highest number of active REs in RS1, we note that FC-active/passive RIS achieves the highest EE and SR. SC-active/passive RIS slightly outperforms SC-active RIS in both cases. FC-active RIS performs slightly worse than the latter RIS variant and slightly better than the former one in terms of EE and SR, respectively. The aforementioned RIS structures significantly outperform the active/active RIS designs; yet, the latter perform substantially better than passive RIS. Also, their performance slowly improves with distance, while the performance of the other RIS variants slowly decreases. As the number of active REs in RS1 is reduced, we observe that the EE of the active/passive RIS variants drops, due to the reduced SR caused by the higher number of passive REs, and eventually the active RIS designs start to outperform them. FC-active/SC-active RIS performs better than hybrid SC-active RIS in terms of EE, when REs' allocation heavily favors SC-active REs. However, both these active/active RIS variants are most energy-efficient when REs' allocation is balanced. We notice the exact same trends for SR, as the number of active REs in RS1 is decreased.

In Figs. 5(a), 5(d), we divide SC-active RIS/RSs in two partitions, such as two PAs are used instead of one, and repeat the previous test. We note that the EE of SC-active RIS slightly improves due to the slightly higher SR, which compensates for

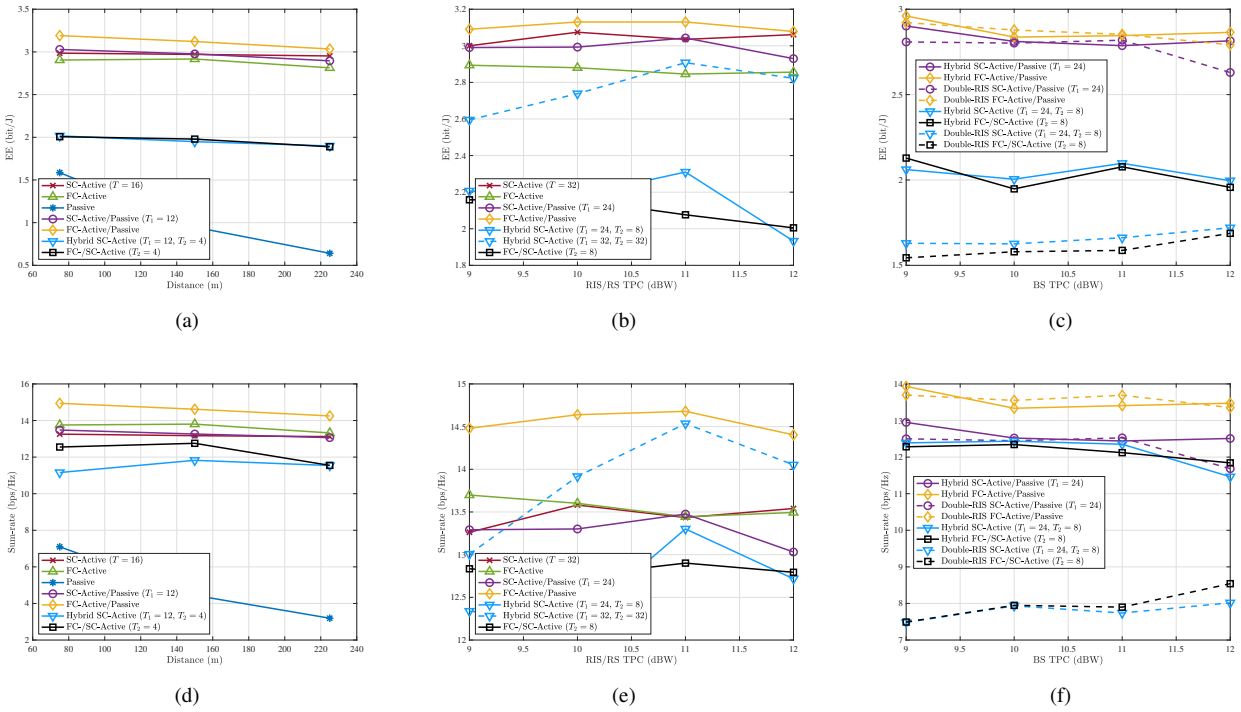

Fig. 5. EE (top) and SR (bottom) vs. distance (left) and RIS (center) or BS (right) TPC budget for different RIS architectures and configurations.

the small increase in the TPC, while the EE of the active/active RIS variants is reduced and slowly drops with distance. In Figs. 5(b), 5(e), we place the users cluster at $(150, 0, 0)$ and vary RIS's TPC budget. We note similar behavior with Fig. 4. We also notice that when we double the number of REs in hybrid SC-active RIS, its EE and SR increase with RIS's TPC budget, until they respectively exceed the EE of FC-active RIS and almost reach the SR of FC-active/passive RIS. After that point, the performance of the hybrid RIS variants starts to decrease, due to diminishing returns caused by the amplification noise which are more pronounced than in the active RIS cases (e.g., because of the smaller number of active REs or the smaller reflect power budget per RS which result in smaller SR). In Figs. 5(c), 5(f), we compare the performance of the hybrid RIS variants against their equivalent double-RIS setups as we vary BS's TPC budget. We notice that the hybrid active/passive RIS variants and their double-RIS equivalent setups substantially outperform their active/active counterparts. The double-RIS active/passive setups perform slightly better than their hybrid equivalents for moderate BS's TPC budget, while for large BS's TPC budget it is the other way around due to the combination of the higher path loss for the remote RIS with limited reflect power budget. Likewise, the hybrid active/active RIS variants significantly outperform their double-RIS equivalents.

VI. Conclusions

In this work, we introduced novel hybrid RIS architectures, analyzed their asymptotic SNR and proposed energy-efficient transmission schemes. Numerical simulations showed that FC-active/passive RIS presents the highest EE, due to its high SR. SC-active/passive RIS follows closely, while consuming less power, and outperforms SC-active RIS. Also, hybrid SC-active RIS can achieve much higher SR than FC-active RIS.

Appendix A
Proof of Lemma 3

The received signal at the user is given by $y = h^* ws + \mathbf{f}_1^\dagger \mathbf{\Phi}_1 \mathbf{z}_1 + n = \widetilde{\alpha}_1 \mathbf{f}_1^\dagger \mathbf{\Theta}_1 \mathbf{g}_1 ws + \mathbf{f}_2^\dagger \mathbf{\Theta}_2 \mathbf{g}_2 ws + \widetilde{\alpha}_1 \mathbf{f}_1^\dagger \mathbf{\Theta}_1 \mathbf{z}_1 + n$. Therefore, the received SNR is written as:

$$\begin{aligned}\gamma_{a/p} &= \frac{\left|\widetilde{\alpha}_1 \mathbf{f}_1^\dagger \mathbf{\Theta}_1 \mathbf{g}_1 w\right|^2 + \left|\mathbf{f}_2^\dagger \mathbf{\Theta}_2 \mathbf{g}_2 w\right|^2}{\widetilde{\alpha}_1^2 \left\|\mathbf{f}_1^\dagger \mathbf{\Theta}_1\right\| \delta_1^2 + \sigma^2} \\ &= \underbrace{\frac{\left|\widetilde{\alpha}_1 \mathbf{f}_1^\dagger \mathbf{\Theta}_1 \mathbf{g}_1 w\right|^2}{\widetilde{\alpha}_1^2 \left\|\mathbf{f}_1^\dagger \mathbf{\Theta}_1\right\| \delta_1^2 + \sigma^2}}_{\gamma_{a/p}^{(1)}} + \underbrace{\frac{\left|\mathbf{f}_2^\dagger \mathbf{\Theta}_2 \mathbf{g}_2 w\right|^2}{\widetilde{\alpha}_1^2 \left\|\mathbf{f}_1^\dagger \mathbf{\Theta}_1\right\| \delta_1^2 + \sigma^2}}_{\gamma_{a/p}^{(2)}}. \end{aligned} \tag{51}$$

The SNR maximization problem is formulated as follows:

$$\text{(SNR1-A):} \quad \max_{w, \widetilde{\alpha}_1, \{\theta_{n,1}\}} \ \gamma_{a/p}^{(1)} \tag{52a}$$

$$\text{s.t.} \quad \text{C7:} \ |w|^2 \leq P_{t,a/p}^{\max}, \tag{52b}$$

$$\text{C8:} \ \widetilde{\alpha}_1^2 \left\|\mathbf{\Theta}_1 \mathbf{g}_1 w\right\|^2 + \widetilde{\alpha}_1^2 N_1 \delta_1^2 \leq P_{r,1}^{\max}. \tag{52c}$$

Using the Lagrange multipliers method, we obtain [20]:

$$w^\star = \sqrt{P_{t,a/p}^{\max}}, \ \theta_{n,1}^\star = \arg\left(f_{n,1}\right) - \arg\left(g_{n,1}\right), \tag{53a}$$

$$\widetilde{\alpha}_1^\star = \sqrt{\frac{P_{r,1}^{\max}}{P_{t,a/p}^{\max} \sum\limits_{n \in \mathcal{N}_1} |g_{n,1}|^2 + N_1 \delta_1^2}}. \tag{53b}$$

By substituting Eq. (53) into $\gamma_{a/p}^{(1)}$, and letting $N_1 \to \infty$, such that $\sum_{n\in\mathcal{N}_1} |f_{n,1}|\,|g_{n,1}| \to N_1 \frac{\pi \varrho_{f_1} \varrho_{g_1}}{4}$, $\sum_{n\in\mathcal{N}_1} |f_{n,1}|^2 \to N_1 \varrho_{f_1}^2$, and $\sum_{n\in\mathcal{N}_1} |g_{n,1}|^2 \to N_1 \varrho_{g_1}^2$, according to the law of large numbers, we obtain

$$\gamma_{a/p}^{(1)} \to N_1 \frac{P_{t,a/p}^{\max} P_{r,1}^{\max} \pi^2 \varrho_{f_1}^2 \varrho_{g_1}^2}{16\left(P_{r,1}^{\max}\delta_1^2\varrho_{f_1}^2 + P_{t,a/p}^{\max}\sigma^2\varrho_{g_1}^2 + \sigma^2\delta_1^2\right)}, \quad (54)$$

which, not surprisingly, is the corresponding asymptotic SNR expression for an active RIS with N_1 REs.

Next, given the optimal solution of SNR1-A and based on Eq. (51), we focus on maximizing the nominator of $\gamma_{a/p}^{(2)}$ subject to the UMC constraints of RS2:

$$\text{(SNR1-B)}: \max_{\{\theta_{n,2}\}} \left|\mathbf{f}_2^\dagger \mathbf{\Theta}_2 \mathbf{g}_2 w^\star\right|^2 \text{ s.t. C9: } 0 \le \theta_{n,2} \le 2\pi. \quad (55)$$

It is easy to verify that $\theta_{n,2}^\star = \arg(f_{n,2}) - \arg(g_{n,2}w^\star)$, $\forall n \in \mathcal{N}_2$ [10]. Then, $\left|\mathbf{f}_2^\dagger \mathbf{\Theta}_2 \mathbf{g}_2 w^\star\right| = \sum_{n\in\mathcal{N}_2} |f_{n,2}|\,|g_{n,2}|$. Therefore, substituting this expression, along with Eq. (53), into $\gamma_{a/p}^{(2)}$, and letting $N_1 \to \infty$ and $N_2 \to \infty$, we obtain

$$\gamma_{a/p}^{(2)} \to N_2^2 \frac{P_{t,a/p}^{\max} \pi^2 \varrho_{f_2}^2 \varrho_{g_2}^2 \left(P_{t,a/p}^{\max}\varrho_{g_1}^2 + \delta_1^2\right)}{16\left(P_{r,1}^{\max}\delta_1^2\varrho_{f_1}^2 + P_{t,a/p}^{\max}\sigma^2\varrho_{g_1}^2 + \sigma^2\delta_1^2\right)}. \quad (56)$$

By adding together Eq. (54) and Eq. (56), as dictated by Eq. (51), we obtain Eq. (15). This concludes the proof.

Appendix B
Proof of Lemma 4

The received signal at the user is given by $y = h^* w s + \sum_{s\in\mathcal{S}} \mathbf{f}_s^\dagger \mathbf{\Phi}_s \mathbf{z}_s + n = \sum_{s\in\mathcal{S}} \widetilde{\alpha}_s \mathbf{f}_s^\dagger \mathbf{\Theta}_s \mathbf{g}_s w s + \sum_{s\in\mathcal{S}} \widetilde{\alpha}_s \mathbf{f}_s^\dagger \mathbf{\Theta}_s \mathbf{z}_s + n$. Thus, the received SNR is written as:

$$\gamma_{a/a} = \frac{\sum_{s\in\mathcal{S}} \left|\widetilde{\alpha}_s \mathbf{f}_s^\dagger \mathbf{\Theta}_s \mathbf{g}_s w\right|^2}{\sum_{s\in\mathcal{S}} \widetilde{\alpha}_s^2 \left\|\mathbf{f}_s^\dagger \mathbf{\Theta}_s\right\| \delta_s^2 + \sigma^2}. \quad (57)$$

The SNR maximization problem is formulated as follows:

$$\text{(SNR2)}: \max_{w,\{\widetilde{\alpha}_s\},\{\theta_{n,s}\}} \gamma_{a/a} \quad (58a)$$

$$\text{s.t.} \quad \text{C10: } |w|^2 \le P_{t,a/a}^{\max}, \quad (58b)$$

$$\text{C11: } \widetilde{\alpha}_s^2 \left\|\mathbf{\Theta}_s \mathbf{g}_s w\right\|^2 + \widetilde{\alpha}_s^2 N_s \delta_s^2 \le P_{r,s}^{\max}. \quad (58c)$$

Using the Lagrange multipliers method, we obtain the optimal solutions, which are given by Eq. (53) by replacing the transmit power budget with $P_{t,a/p}^{\max}$ and the index of RS1 with that of RS s. By substituting these expressions into $\gamma_{a/a}$ and letting $N_s \to \infty$, we obtain Eq. (17). This concludes the proof.

References

[1] S. Gong *et al.*, "Towards Smart Wireless Communications via Intelligent Reflecting Surfaces: A Contemporary Survey," *IEEE Commun. Surv. Tut.*, vol. 22, no. 4, pp. 2283–2314, 2020, fourthquarter.

[2] Q. Wu, S. Zhang, B. Zheng, C. You, and R. Zhang, "Intelligent Reflecting Surface Aided Wireless Communications: A Tutorial," *IEEE Trans. Commun.*, vol. 69, no. 5, pp. 3313–3351, May 2021.

[3] C. Huang, A. Zappone, G. C. Alexandropoulos, M. Debbah, and C. Yuen, "Reconfigurable Intelligent Surfaces for Energy Efficiency in Wireless Communication," *IEEE Trans. Wireless Commun.*, vol. 18, no. 8, pp. 4157–4170, Aug. 2019.

[4] K. Zhi, C. Pan, H. Ren, K. K. Chai, and M. Elkashlan, "Active RIS Versus Passive RIS: Which is Superior With the Same Power Budget?" *IEEE Commun. Lett.*, vol. 26, no. 5, pp. 1150–1154, May 2022.

[5] C. You and R. Zhang, "Wireless Communication Aided by Intelligent Reflecting Surface: Active or Passive?" *IEEE Wireless Commun. Lett.*, vol. 10, no. 12, pp. 2659–2663, Dec. 2021.

[6] K. Liu, Z. Zhang, L. Dai, C. Xu, and F. Yang, "Active Reconfigurable Intelligent Surface: Fully-Connected or Sub-Connected?" *IEEE Commun. Lett.*, vol. 26, no. 1, pp. 167–171, Jan. 2022.

[7] Z. Kang, C. You, and R. Zhang. (2022, Jul.) Active-Passive IRS aided Wireless Communication: New Hybrid Architecture and Elements Allocation Optimization. arXiv preprint. [Online]. Available: https://arxiv.org/pdf/2207.01244.pdf

[8] X. Yu, D. Xu, and R. Schober, "MISO Wireless Communication Systems via Intelligent Reflecting Surfaces," in *IEEE/CIC Int. Conf. Commun. in China (ICCC)*, Changchun, China,, Aug. 2019, pp. 735–740.

[9] S. Zhang and R. Zhang, "Capacity Characterization for Intelligent Reflecting Surface Aided MIMO Communication," *IEEE J. Sel. Areas Commun.*, vol. vol. 38, no. 8, pp. 1823–1838, Aug. 2020.

[10] Q. Wu and R. Zhang, "Intelligent Reflecting Surface Enhanced Wireless Network via Joint Active and Passive Beamforming," *IEEE Trans. Wireless Commun.*, vol. 18, no. 11, pp. 5394–5409, Nov. 2019.

[11] X. Yu, D. Xu, D. W. K. Ng, and R. Schober, "IRS-Assisted Green Communication Systems: Provable Convergence and Robust Optimization," *IEEE Trans. Commun.*, vol. 69, no. 9, pp. 6313–6329, Sep. 2021.

[12] Q. Wu and R. Zhang, "Beamforming Optimization for Wireless Network Aided by Intelligent Reflecting Surface With Discrete Phase Shifts," *IEEE Trans. Commun.*, vol. 68, no. 3, pp. 1838–1851, Mar. 2020.

[13] G. Zhou, C. Pan, H. Ren, K. Wang, M. Di Renzo, and A. Nallanathan, "Robust Beamforming Design for Intelligent Reflecting Surface Aided MISO Communication Systems," *IEEE Wireless Commun. Lett.*, vol. 9, no. 10, pp. 1658–1662, Oct. 2020.

[14] K. Ntougias and I. Krikidis, "Probabilistically Robust Optimization of IRS-aided SWIPT Under Coordinated Spectrum Underlay," *IEEE Trans. Commun.*, vol. 70, no. 4, pp. 2298–2312, Apr. 2022.

[15] C. Huang, A. Zappone, M. Debbah, and C. Yuen, "Achievable Rate Maximization by Passive Intelligent Mirrors," in *IEEE Int. Conf. Acoust., Speech and Signal Process. (ICASSP)*, Apr. 2018, pp. 3714–3718.

[16] H. Guo, Y.-C. Liang, J. Chen, and E. G. Larsson, "Weighted Sum-Rate Maximization for Intelligent Reflecting Surface Enhanced Wireless Networks," in *IEEE Global Commun. Conf. (GLOBECOM)*, Waikoloa, HI, USA, Dec. 2019.

[17] M.-M. Zhao, Q. Wu, M.-J. Zhao, and R. Zhang, "Exploiting Amplitude Control in Intelligent Reflecting Surface Aided Wireless Communication with Imperfect CSI," arXiv: 2005.07002, May 2020.

[18] R. Long, Y. Liang, Y. Pei, and E. G. Larsson, "Active Reconfigurable Intelligent Surface Aided Wireless Communications," *IEEE Trans. Wireless Commun.*, vol. 20, no. 8, pp. 4962–4975, Aug. 2021.

[19] D. Xu, X. Yu, D. W. Kwan Ng, and R. Schober, "Resource Allocation for Active IRS-Assisted Multiuser Communication Systems," in *Asilomar Conf. Signals, Syst., Comput.*, 2021, pp. 113–119.

[20] Z. Zhang *et al.*, "Active RIS vs. Passive RIS: Which Will Prevail in 6G?" *IEEE Trans. Commun.*, 2023, Early Access.

[21] N. T. Nguyen *et al.*, "Hybrid Active-Passive Reconfigurable Intelligent Surface-Assisted UAV Communications," in *IEEE Global Commun. Conf. (GLOBECOM)*, Rio de Janeiro, Brazil, Dec. 2022.

[22] ——, "Fairness Enhancement of UAV Systems with Hybrid Active-Passive RIS," *IEEE Trans. Commun.*, 2023, Early access.

[23] W. Lyu, Y. Xiu, S. Yang, C. Yuen, and Z. Zhang, "Energy-Efficient Cell-Free Network Assisted by Hybrid RISs," *IEEE Wireless Commun. Lett.*, vol. 12, no. 4, pp. 718–722, Apr. 2023.

[24] A European Green Deal: Striving to be the first climate-neutral continent. Online. [Online]. Available: https://commission.europa.eu/strategy-and-policy/priorities-2019-2024/european-green-deal_en

[25] K. Shen and W. Yu, "Fractional Programming for Communication Systems—Part I: Power Control and Beamforming," *IEEE Trans. Signal Process.*, vol. 66, no. 10, pp. 2616–2630, May 2018.

[26] X. He and J. Wang, "QCQP With Extra Constant Modulus Constraints: Theory and Application to SINR Constrained Mmwave Hybrid Beamforming," *IEEE Trans. Signal Process.*, vol. 70, pp. 5237–5250, Oct. 2022.